Title
Nano-patterned Biopolymer Substrate for Ophthalmic Device

Author
Luo, Jingyi

Publication Date
2021

UNIVERSITY OF CALIFORNIA,
IRVINE

Nano-patterned Biopolymer Substrate for Ophthalmic Device

THESIS

submitted in partial satisfaction of the requirements
for the degree of

MASTER OF SCIENCE

in Materials Science and Engineering

by

Jingyi Luo

Thesis Committee:
Professor Albert F. Yee, Chair
Professor Xiaoqing Pan
Professor James V. Jester

2021

TABLE OF CONTENTS

LIST OF FIGURES

LIST OF TABLES

ACKNOWLEDGMENTS

I would like to thank my advisor, Prof. Albert F. Yee, for his treasured supports and guidance throughout my project. I truly appreciate every feedback, critiques and trust that he always generally provided. My gratitude extended to my co-advisor, Prof. Xiaoqing Pan, and committee member, Prof. James V. Jester, for the providing learning opportunities which were influential in my studies. I would also like to thank Prof. Han Li, Prof. Alon Gorodetsky, Prof. Wendy Liu and Prof. Eric Pearlman for supporting my project by providing the laboratory space and equipment. I also want to thank all my amazing former and present colleagues, Xin Fu, Sara Heedy, Yasaman Fatapour, Michaela Strasser, Junming Cai and Rachel Rosenzweig, for the valuable suggestions and discussions all through my project. This project will not be possible without the support and funding from the Peer Reviewed Medical Research Program (PRMRP).

ABSTRACT

Nano-patterned Biopolymer Substrate for Ophthalmic Device
by
Jingyi Luo
Master of Science in Materials Science and Engineering
University of California, Irvine, 2021
Professor Albert F. Yee, Chair

Approximately 2 million cases of microbial keratitis occur in the world every year. Microbial keratitis can develop into vision loss and other severe complications. The current treatment is the use of antibiotic eye drops, which have diminished effect due to the increasing development of antimicrobial resistance. Instead of using drugs to control microbe growth, we engineered an antimicrobial nanopillared topography onto a hydrogel material to physically inhibit microbe growth and reduce the risk of contact lens-related microbial keratitis. The challenges, thus objective of this research, is to develop a method to integrate the nanotopography onto curved lens surfaces and to stabilize the nanostructures by crosslinking the hydrogel polymer. The hydrogel chitosan has antimicrobial and mucoadhesive properties that can promote wound healing. The dimensions and curvatures of the lens need to be controllable after the material is saturated with solvent. Chitosan hydrogels are stabilized by co-crosslinking with a covalent crosslinker, genipin (GP), and ionic crosslinker, tripolyphosphorous (TPP), or single crosslinking with only TPP. The material properties are modulated and characterized to suit the contact lens application. The antifungal properties of the engineered contact lens are also characterized with *in vitro* test. The result shows that the resulting ophthalmic device is able to stabilize the nanotopography and hinder *Fusarium oxysporum* growth on the device surface for 24 hours.

Chapter 1: Introduction

Cell-material interaction is normally controlled by characteristics like surface composition, surface charge, and wettability. It is also important to highlight the influence of physical characteristics of material surface in the nano- and micro-scale on cell behavior. Physical interactions between the biological system and material surface offer opportunities to improve and develop therapeutic efficacy of medical devices. This interaction has been studied and utilized for cell and microbe adhesion control. In the field of tissue engineering, extracellular matrix (ECM) provides natural support and guidance for cell proliferation. Cell-substrate interaction at the interface, in particular, has attracted the attention of many researchers in recent years.[1] Nanopatterned surfaces have been researched as functional templates for regulating cell growth on nanomaterials. For example, the ability of fibroblast to proliferate was observed to be limited on the micro pillared surfaces.[2] Morphology of mammalian cells has also been varied between surfaces with different micro-pillar periodicities and sizes. This observation is also seen with other types of cell systems such as bacteria and fungi. Several studies have shown that bacteria and fungi growth can be inhibited on nanopillared surfaces which mimics the nanostructure on cicada and dragonfly wings.[3, 4] Surface topography not only can influence the cell behavior by guiding the cell proliferation but also by varying factors like hydrophobicity, electrostatic interactions, and van der Waals forces.[5]

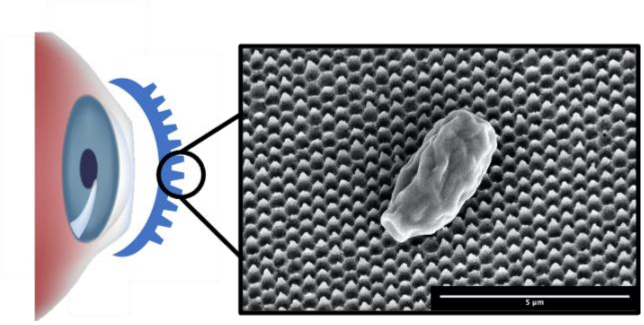

Figure 1: Hydrogel Contact Lens with nanopillared surface for enhanced antimicrobial properties.

In this thesis work, a nano-fabrication technique is applied to the biopolymer, chitosan (CS), to produce nanopillar topography to enhance antimicrobial properties. A nanopillar topography is designed for the ophthalmic device surface for eliminating fungi adhesion and biofilm growth while retaining optical functions. (Figure 1) The goal of this research is to design the optimal manufacturing process and tune the material properties to some criteria for specific applications. For ophthalmic devices like contact lenses, the selected material must have the following desirable properties: high wettability, low surface friction, and high transparency. In order for polymer to retain the surface modification, the mechanical properties of the material have to be tunable using a chemically or ionically crosslinking process. The proposed material for this project is chitosan, which is a polysaccharide found abundantly in nature. Unlike common contact lens materials like 2-hydroxyethyl methacrylate (HEMA), chitosan is more hydrophilic and known to have bacteriostatic properties. Chitosan hydrogel has been extensively studied as a nanomaterial in the field of drug delivery systems due to its antimicrobial properties, good biocompatibility, and nematic ordering behavior.[6] It is also known that chitosan can be chemically modified to produce favorable properties and functions.[7]

1.1 Contact Lens Related Microbial Keratitis

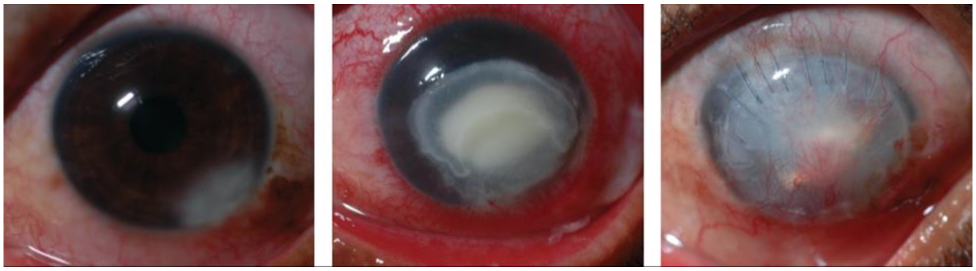

Figure 2[8]: Fusarium infected cornea with 3 months of fungal keratitis development. The fungi eventually penetrated the cornea and the patient had to receive keratoplasty.

The two common procedures used to treat astigmatism, nearsightedness, and farsightedness surgically, laser epithelial keratomileusis (LASEK) and photorefractive keratectomy (PRK), result in corneal surface tissue ablation. The healing process of the cornea after such refractive surgery or trauma requires minimal external irritation; therefore, a bandage contact lens must be applied to the wound immediately after surgery. This therapeutic lens protects the wound surface against abrasion from the shear movement of the eyelids, which can cause the epithelial flap to deteriorate, enlarging the area of wound exposure to the environment and leading to a higher risk of microbial keratitis. The eye's healing process will slow due to these additional complications from external irritations to the wound.

Therapeutic contact lenses are usually used to manage corneal disorder, prevent post-surgical complications to the eye, and promote regeneration of the corneal epithelium. The abrasion caused by eyelid shear motion on the cornea will increase the discomfort and pain for the patient. The bandage contact lens will also reduce the risk of striae (flap folding) and scar tissue formation.[9] Another major complication for therapeutic contact lens wearers is microbial keratitis, which is a serious sight-threatening condition due to the growth of bacteria or fungi on the surface of the cornea. When microorganisms enter the cornea and accumulate at the wound bed from the surrounding environment or contact lens, these invading organisms can penetrate the cornea and cause irreversible damage. Regardless of surgery, contact lens wear is one of the top predisposing factors for microbial keratitis and corneal infection.[10] The risk of microbial keratitis is higher for long-term use contact lens wearers.[10] Overnight wear of bandage contact lenses can significantly inhibit oxygen transmission to the cornea, thereby slowing the corneal epithelial healing process. Mauger et al. analyzed the effect of oxygen concentration on the corneal epithelium healing process and found that higher oxygen concentration can induce healing of corneal abrasions.

Therapeutic contact lenses can reduce the oxygen at the corneal surface which can predispose the eyes to infection.[11] For the lens to be worn long-term, the essential properties for bandage contact lens material are high oxygen permeability, good biocompatibility, and resistance to protein deposition. Common materials used in today's lens fabrication technologies are poly (hydroxyethyl methacrylate) (pHEMA), silicone hydrogels, and collagen shields.[12,13] These materials can also be copolymerized or composited to achieve a combination of desired properties.

1.2 Methods to Control Fungal Growth on Medical Device Surface

The bandage contact lens can increase the risk of microbial keratitis caused by contaminations during transferring process and limited immune response due to low oxygen permeability. The major agents that cause fungal keratitis are *Aspergillus*, *Fusarium,* and *Candida* species which are commonly found in the environment.[14] Eye drops containing antifungal drugs are the most common treatment prescribed by the ophthalmologist to prevent infections when a patient experiences eye trauma or is using bandage contact lenses. Eye drops are inefficient as the drug gets washed away quickly by dynamic tear films. Therefore, continual application is required when treating a condition with eye drops. This can lead to low patient compliance which will delay or worsen the treatment.

Nowadays, the extensive use of antibiotics induces increasing antimicrobial resistance, therefore reduces the effectiveness of the medication. Moreover, fungi pathogens can produce a polysaccharide matrix called biofilm that serves as a protective shield for microcolonies to resist antifungal therapy.[15] Zhang et al. found that fungal biofilm formation undergoes four main stages: adhesion, germling formation, microcolony formation, and biofilm maturation.[16] A physical antimicrobial method using surface nanotopography to control fungi from the first stage of biofilm formation is researched by many scientists all over the world. The nanopillar topography inspired from cicada wing surface structures exhibits an antimicrobial effect towards some bacteria and fungi strains.[5, 17] However, the mechanism of this phenomenon is still controversial. Researchers have suggested that the nanopillars are microbicidal by applying mechanical stress to the cell and causing physical stretching of the microbe cell membrane, which leads to cell rupture.[17, 18] The pillar sharpness and spacing also have an effect on the antimicrobial performance of the nanostructured surface. Rosenzweig et al. found that greater pillar periodicity (~500 nm) exhibit better antifungal effect when comparing to pillar periodicity of 200 nm and 300 nm.[3] In the paper, she also claims that the fungicidal effect can be a result of the interaction between nanopillars and mechanosensitive protein on the cell membrane, which influences cell growth and metabolism. The effectiveness and timing of treatment are significant in preventing future complications for corneal trauma. Accordingly, these biomimetic nanopillar structures are incorporated into the design of bandage contact lenses to work as the first barrier to prevent fungal adhesion and potential fungal keratitis.

Chapter 2: Vacuum Forming Method for Molding Nanopatterns on Curved Surfaces

2.1 Objective

Soft contact lenses can be produced by Lathe cutting, spin casting, and cast molding methods. Spin casting is a method using centripetal force to form polymer into curved contact lenses. The base curvature of the lens is determined by the shape of the negative mold. Rotational speed and volume of polymer solution are two factors used to regulate center lens thickness. The edge thickness of the lens is an essential factor in contact lens design and can be altered by controlling rotation speed during spin casting. Thinner edge results in better lens fitting and less influence by the friction of the eyelid.[19] This method has high accuracy in controlling the geometry of contact lenses and is feasible for molding texture onto the exterior side of the lens. Spin cast lenses only contain one base curvature therefore the negative mold should match the aspheric profile of the cornea.[20] To incorporate nanotopography to the front side of the contact lens, the negative mold used for spin casting needs to be modified using the replica molding method. Replica molding is a technique commonly used in polymer lithography to reproduce nano- and micro-scale patterns. It is an effective method for molding mechanically soft gel and film as it can duplicate the spatial pattern in a single step. The replication used in this study encompasses three steps: Firstly, a negative mold is obtained via nanoimprint mold material onto a metal nanotextured positive mold, then followed by forming the negative mold into desired lens dimensions and shape using vacuum force. Finally, the contact lens is cast material onto the negative mold.

The objective of this chapter is to describe the replication of the nanopillar topography and design of a manufacturing process for making lens-shaped nanoholed negative mold. As introduced in Chapter 1, the nanopillar surface inspired by cicada wing topography shows physical antimicrobial properties. Both Heedy et al. and Rosenzweig et al. showed that pillars with 500 nm periodicity have the most optimal antifungal effect compared with flat surfaces or those with smaller periodicity. [3, 21] Hence, a commercially available nanopillared nickel substrate with pillar periodicity of 500 nm and pillar height ~700 nm is used as the positive mold for replication.

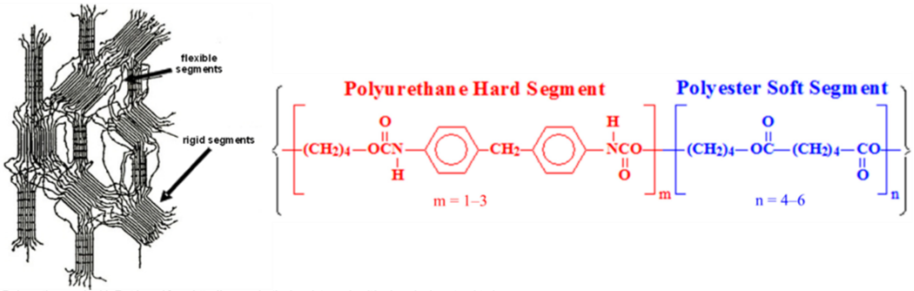

Polyurethanes. (n.d.). Retrieved from http://www.whatischemistry.unina.it/en/maglpolyuretan.html

Figure 3[22]*: Molecular structure of polyurethane including the hard and soft segments. The hard segments form into rigid blocks by aligning the polymer chains.*

In the first step of replication, the thermoplastic elastomer, polyurethane (PU), is used as the negative mold material for the hot embossing nanoimprinting. PU is a biocompatible synthetic material with high versatility and is commonly used in thermal molding. The molecular structure of PU is composed of two alternating polymer blocks: flexible and hard segments. (Figure 3) The flexible segments contain polyester or polyether sequences whereas the hard segments include di-isocyanates and low molecular weight polyols.[23] The hard segments aggregate to form a micro-phase which is dispersed in the soft segments. Therefore, the properties of PU are dependent on the ratio between the flexible and hard segments and their phase structure. The two types of PU used in this study are commercially available 72D and 70A thermoplastic PU. The numbers and letters represent the shore hardness of polyurethane, whereas Shore A is softer than Shore D. The hardness of polyurethane depends on the amount of hard and soft segments within the PU copolymer blocks. The glass transition and melting temperature (T_g and T_{melt}) for PU are not defined and can vary depending on the specific segments' ratio and phase structure. As a reference, the T_g is observed between 70°C - 120°C and T_{melt} is 180°C - 200°C according to Lu et al. and Koberstein et al.[24, 25]

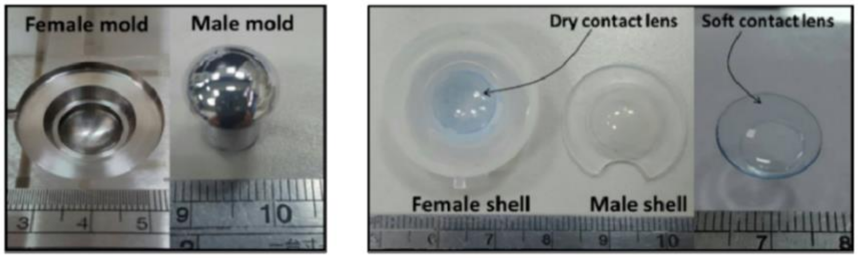

a) b)

Figure 4[25]: The injection molds for shell molds shown in (a). The shell mold for casting soft contact lens (b).

Normally, the contact lens negative mold is made by injection molding from metal injection molds to obtain the lens shape. (Figure 4) Customizing metal injection molds with nanotopography is not cost-effective for this research and inconvenient if there is a need for alternation of lens dimensions. In consequence, a vacuum forming method is used to create a lens-shaped negative mold with interior nanotopography. The process includes softening the mold by increasing the temperature to above PU T_g (>120°C) and assisted with solvent-driven deformation previous to vacuum forming. Then vacuum force was used to deform the PU negative mold and the mold PU mold was confined by a three-dimensional (3D) printed vacuum chamber. By incorporating stacking layers of rigid 72D PU and soft 70A PU, the flexibilities of mold were optimized to induce the next step of reshaping mold. Rigid 72D PU was used to stabilize the nanotopography during replication and mold deformation while 70A PU acts as a flexible backing for the negative mold. The interface between two PU layers acts like a barrier to minimize the solvent effect on the nanotopography. The vacuum chambers were designed using the modeling software SolidWorks and printed with Ultimaker^3 3D printer. The rabbit cornea that the contact lens must fit for the following animal studies has a base curvature of 8.65mm and a diameter of

15.50 mm.[27] The dimensions and curvature of spherical cap-shaped confinement within the vacuum chamber were designed based on these dimensions. Polylactic acid (PLA) was used as construction material for the 3D printed vacuum chamber (Figure 6. c), and polyvinyl alcohol (PVA) was used to support the print. Then PVA supports were dissolved in water to create vacuum channels in the vacuum chamber. The lens dimension can be altered easily by 3D printing based on the lens material swelling behavior to fit the cornea.

The nanostructures on nanoprinted negative mold and lens shape negative mold were evaluated by scanning electron microscopy (SEM) and atomic force microscopy (AFM). The assumption is that the nanotopography on PU negative lens mold is reproducible and has little effect from the vacuum forming process. The resulting nanotopography on the molded lens surface was verified by SEM.

2.2 Experimental Procedure

2.2.1 Solution preparation

Polyurethane (PU, Texin®) solution (10wt%) was obtained by dissolving 1g of PU pellet in 9g of 100% dimethylformamide (DMF, Fisher Chemical) at 70°C for overnight until the solution is homogeneous. Both 72D and 70A PU solutions were prepared at the same concentration of 10 wt%. The solvent used to soften PU films contains 50vol% of DMF in Mili Q water. The exothermal reaction between water and DMF will generate heat, therefore a secondary container is required for safety purposes. All actions need to be carried out in the fume hood due to the possible carcinogenicity of DMF.

2.2.2 Nanoholed negative mold preparation

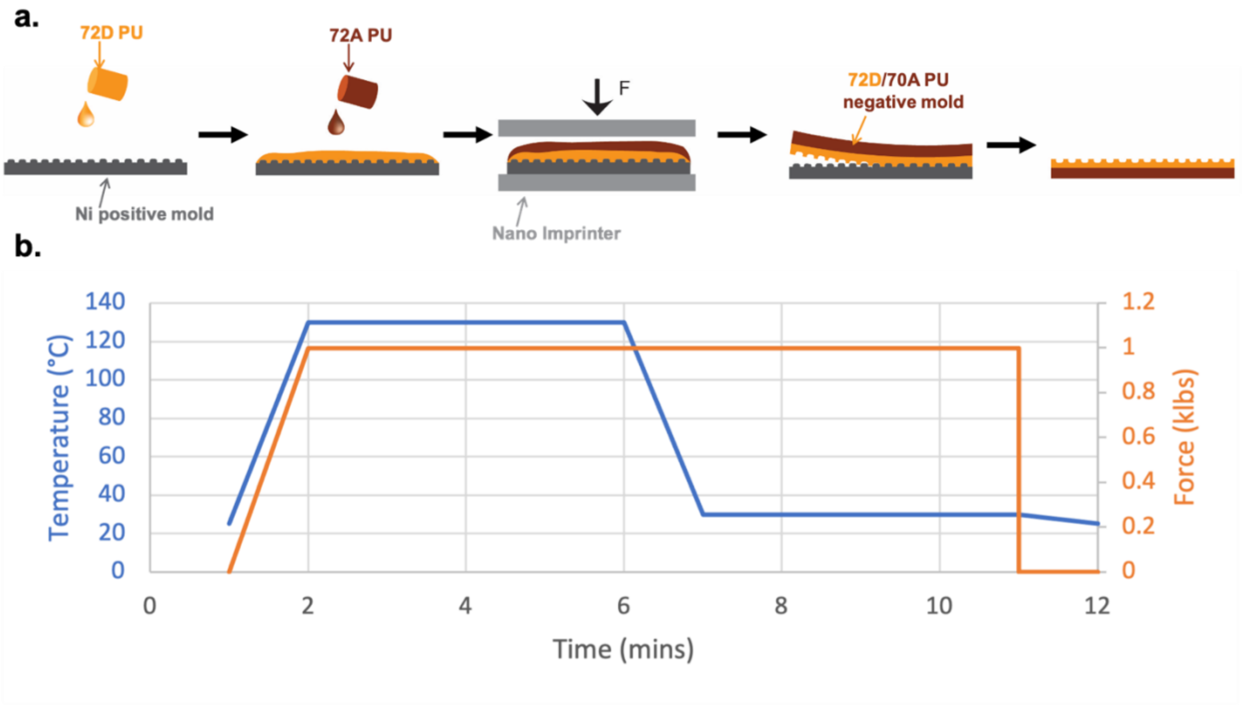

Figure 5: (a) Schematic of fabrication of 2D nanostructured PU negative mold replicating the nanotopography on the Ni positive mold. (b) Schematic correlation between temperature and applied force overtime during nanoimprinting.

The two layers of PU molds were prepared on a 20 mm x 20 mm Ni nanopillar substrate (Temicon, Germany), which was used as the positive mold. The pillar structures are referred to as P500 according to their 500 nm pillar periodicity. 600 µl of 10wt% 72D PU solution was first cast onto the Ni nanopillared substrate and left to dry at 80°C for 1hr. Then the same amount of 10wt% 70A PU solution was cast on top of the dried 72D PU layer to attain a 1:1 ratio layer. Once the two-layered PU negative mold was completely dried, which usually takes at least 3-5 hours, the mold was then compressed in the nanoimprinter (Tetrahedron). (Figure 5, a) The optimal program for nanoimprinting was first to increase the temperature of PU to 130°C, which is above reported T_g and below T_{melt}, and then 1.0 klbs force was applied to the negative mold on Ni substrate for 5 minutes to flow PU into the gap between nanopillars. (Figure 5, b) Lastly, the temperature was lowered to 30°C without changing the force and held for 5 minutes to stabilize the nanoholed structure on the negative mold. As the last step, the negative nanoholed PU mold was peeled off from the P500 Ni substrate. This PU nanoimprinting method was developed by previous master student Junming Cai from Prof. Albert Yee's group.

2.2.3 Vacuum formation of lens shaped negative mold

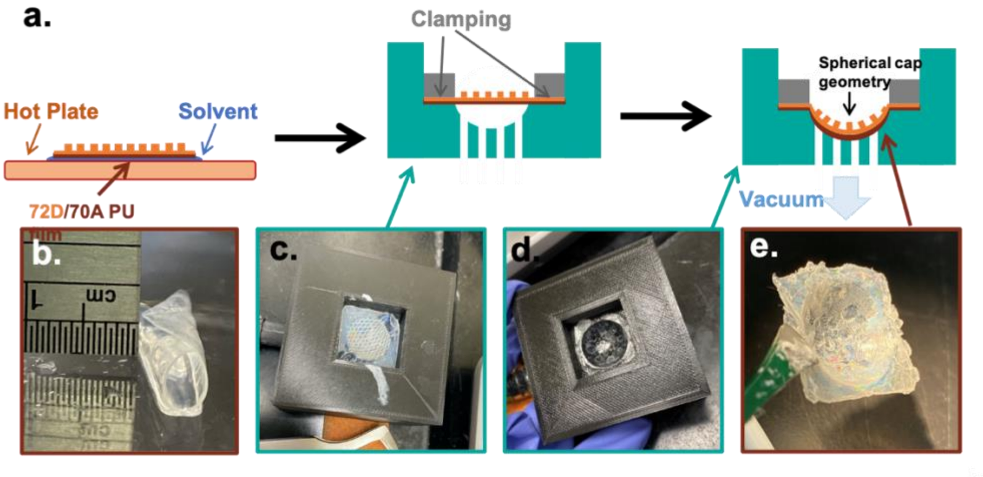

Figure 6: (a) Schematic diagram of the vacuum forming process of the PU negative mold. (b) The nanoimprinted PU negative mold is softened with 50% DMF. (c,d) 3D printed vacuum forming chamber. The spherical cap-shaped single-surface mold is used to guide the shape of PU mold when applying vacuum pressure. (e) The nanoholed PU lens mold after vacuum forming.

Before vacuum forming, the nanoholed negative PU mold was softened to a degree where the mold can deform easily into the lens shape. To minimize deformation of the nanoholed topography, only the flat side, which faces away from the nanotopography, of the negative PU mold was in contact with the 50 vol% DMF solvent. The solvent was first dropped onto a glass petri dish on the hotplate, followed by placing PU negative mold with the flat side down on the solvent droplet. The PU negative mold needs to lay flat on the glass petri dish for even heat distribution. This was achieved by applying force at the four corners of the PU negative mold to hold the film down. The temperature of hotplate was maintained at 80 °C throughout the softening process and the solvent was added every 5 minutes to prevent drying of the PU negative mold. After 20 minutes of softening, the PU negative mold was placed in the vacuum chamber with four sides clamped. The vacuum force (1 atm) was slowly applied to the softened PU negative mold for deformation. A metal mesh was inserted between the PU negative mold and vacuum channels to smooth the surface of the lens-shaped PU negative mold. Figure 7 shows the difference in mold surface smoothness with or without the metal mesh insert. After experimenting with different mesh sizes and materials, the optimal metal mesh is the pure copper mesh (First Automation Inc.) with 0.1 mm mesh size. The lens-shaped PU negative mold can be acquired after at least 24 hours of applying vacuum pressure.

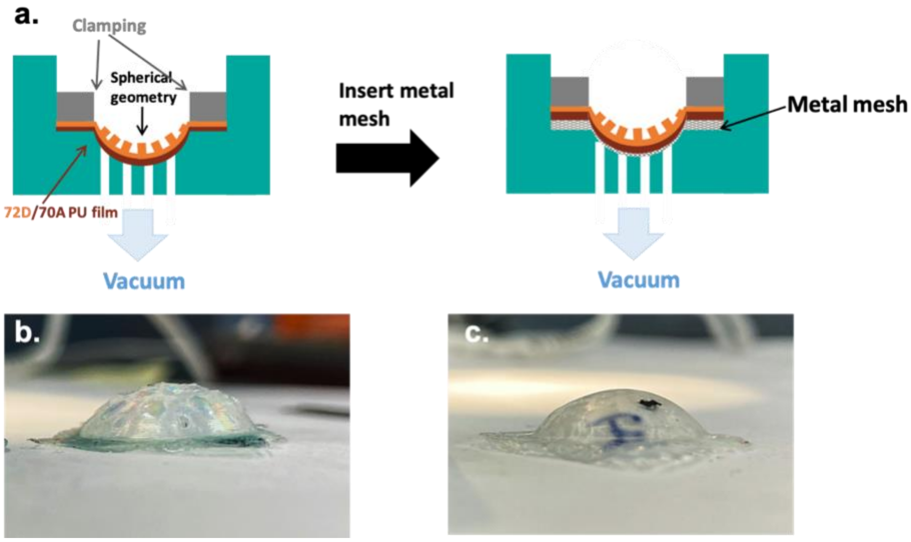

Figure 7: The vacuum forming system consolidates a layer of metal mesh to improve the smoothness of the curved mold surface.

2.3 Characterization

2.3.1 Scanning Electron Microscopy

The nontopography of imprinted PU negative mold was imaged by scanning electron microscope (SEM) to evaluate if the nanohole structures are uniform and reproducible. The SEM images were taken using the FEI Magellan SEM with an electron voltage of 5 kV and an electron current of 23.7 pA. The SEM samples were coated with 4 nm platinum/palladium (Pt/Pd) coating using a LEICA 200 sputter coater before SEM imaging to increase resolution and minimize the electron charging effect. Both the sputter coater and SEM are located at the Irvine Materials Research Institute (IMRI) in UC Irvine.

2.3.2 Atomic Force Microscopy

The nanoholed structures on both the PU negative mold and lens-shaped PU negative mold were characterized using atomic force microscopy (AFM) to assess the depth of nanoholes. A monolithic silicon probe (NanoWord Pointprobe® 320kHz) with aluminum coating is used to scan samples with tapping mode. The pillar cross-section profile was analyzed using Gywddion software and maximum pillar heights are identified using Matlab.

2.4 Result and Discussion

2.4.1 Scanning Electron Microscopy characterization

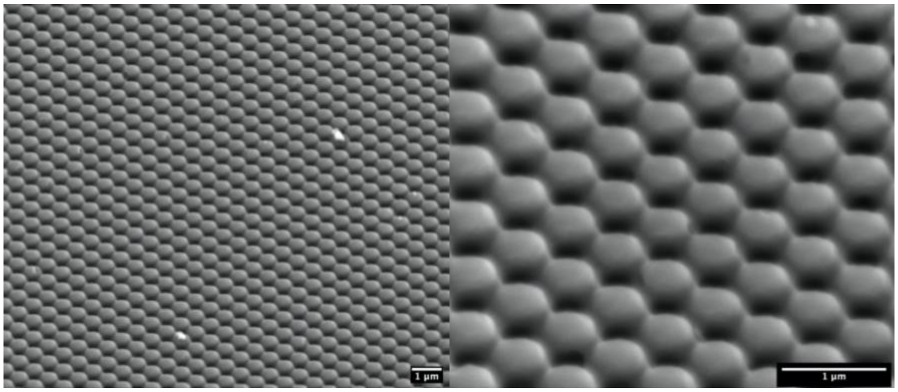

Figure 8: SEM images that demonstrate the nanoholded surface on a negative lens mold. The scale bar is 1 μm.

The negative mold transfers nanopillar structures by filling PU into spacings between pillars and pressed on the Ni positive mold. The moldability of PU polymer increases when temperature reaches 130°C during imprinting. The curing process was finished by slowly decreasing the temperature of PU to room temperature. Using this process, the PU negative mold will form nanoholes which are inverse structures of nanopillars on the positive mold. These nanohole structures on the nanoimprinted PU negative mold were visualized using SEM. As shown in the SEM nanographs, the nanohole structures are homogeneous, which demonstrates that the nanopillars from Ni mold are successfully transferred onto the PU negative mold. This shows 72D PU has enough rigidity to prevent collapse of nanohole structures. The PU negative mold was then peeled off from the Ni positive mold without leaving residue material on the positive mold. PU's good resistance to acids is essential for stabilizing nanohole structures when casting contact lens material, which was dissolved in acetic acid. The nanopillar structures from Ni positive mold have a high aspect ratio and high feature density. Therefore, the nanohole mold was further characterized with AFM to quantify the depth and cross-section shape of the nanoholes.

2.4.2 Atomic Force Microscopy characterization

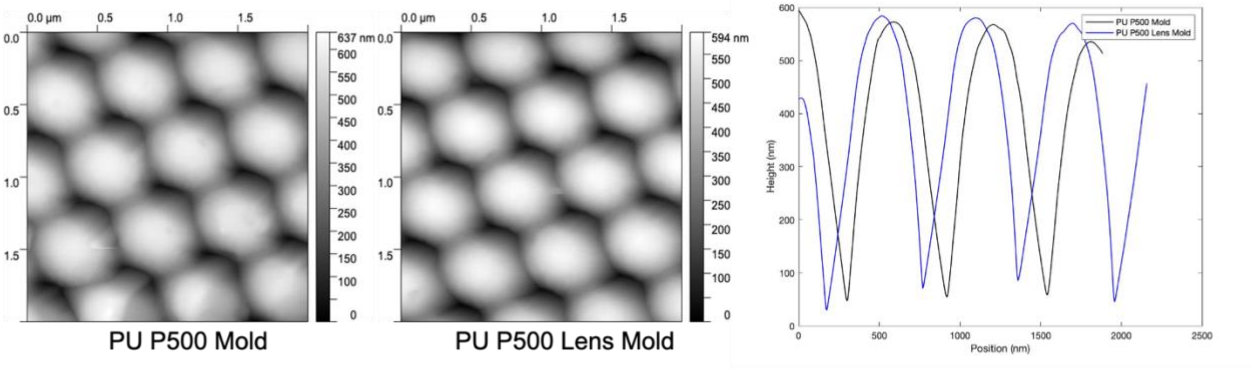
PU P500 Mold

PU P500 Lens Mold

Figure 9: Representative AFM scans of nanoholes on the PU molds. The cross-section profile is analyzed using Gywddion.

To investigate if the vacuum forming method will damage the nanohole structures on PU negative mold, the topography of both negative molds was scanned using AFM. The cross-section of the nanohole structures was analyzed using Gywddion and plotted using Matlab. The z-height was normalized to only show the depth of nanotopography without the full thickness of the PU mold for more accurate readings. The left two AFM images in Figure 9 demonstrate that both PU negative mold and lens-shaped negative mold attained uniform nanohole structures. This proves that the solvent-driven deformation and vacuum forming process only change the macroscopic shape of PU negative molds and have little effect on nanohole structures. The cross-section profile of nanoholes is shown in the graph on the right-hand side of Figure 9. One can see that the nanoholes on the two molds are similar in depth (~600 nm) and geometry. The shift in position is due to the difference in scanned area and nanohole arrangement in that area. The average depth of nanopillars on the positive Ni mold is around 700 nm which is higher than the depth observed here. The pyramid-shaped cantilever tip could prevent the entire tip to reach the bottom of the features. This is verified in the next chapter where the hydrogel nanopillars molded from these PU negative molds show greater depth than 600 nm.

Chapter 3: Fabrication of Nanopatterned Contact Lens for Antibacterial Purpose

3.1 Objective

Microbial keratitis is a severe disease that could cause blindness and potentially require enucleation of the eye. Fungal keratitis is a major global health problem, particularly in developing countries. Any type of corneal trauma can promote pathogens entry to the cornea and growth in the stroma which leads to keratitis.[28] The rapid disease progression limits the current drug delivery method, which is the use of antifungal eyedrops with continuous application. The eyedrops have a low corneal penetration rate due to the fast tear flow cycle. Additional antifungal approaches need to be established to prevent fungal keratitis at an early stage. In this chapter, my approach using a nanostructured surface to hinder fungi attachment and growth mechanically is presented. This antifungal surface is composed of nanoscaled pillars that are inspired by the surface structures on the membranous area of cicada wings. The highly ordered nanopillars on cicada wings have been researched for their microbiocidal properties. Román-Kustas et al. have shown that the topography of cicada wings plays a key role in antimicrobial functionality.[29] Heedy et al. also show that replicated nanopillared surface on hydrogel material still maintains antimicrobial properties.[21] In this chapter, a contact lens with nanopillared exterior surface is designed as a first-aid shield to prevent fungi entry and attachment to the corneal wound.

Oxygen permeability and mechanical strength are two of the most important factors that determine the performance of contact lenses. The comfort and durability of contact lenses depend heavily on these two factors. By comparing with commercially available contact lens, the designed chitosan contact lens should reach a mechanical modulus of 3 MPa along the plane of the lens. Ashkan Aryaei et al. showed that the modulus of crosslinked chitosan hydrogel can reach 6.3 MPa.[30] Besides comfort to the wearer, mechanical properties are also important for the stability of nanopillars on the surface to prevent their collapse at the swollen state. Tensile properties are obtained by testing of hydrated chitosan strips with tensile tester. The Young's modulus for material can be determined by the slope of the linear region in the initial part of the stress vs. strain curves. The desired oxygen permeability for contact lens is desired to be within the range of 60 - 140 (10^{-11} cm^2*ml_{O2})/ ($s*ml_{Lens}*mm$ Hg). In this work, due to the limitation of equipment, the oxygen permeability is indirectly represented instead by the swelling ratio. as Komiyama et al. asserted. They found that the oxygen permeability of conventional hydrogel increases when the water content of the swollen membrane rises.[31] A hydrogel contact lens with high water content will allow more oxygen to reach the cornea through the water in-between the porous networks. Materials with low oxygen transmissivity can cause contact lens-induced dry eye (CLIDE). But high-water content hydrogel contact lens is often not suitable for patients with dry eye syndrome, because such materials can draw out tears that would have been available, resulting in dehydrating the eye which leads to more severe complications.[32] Conventional hydrogel contact lenses obtain water content range from 38% to 70%.[33]

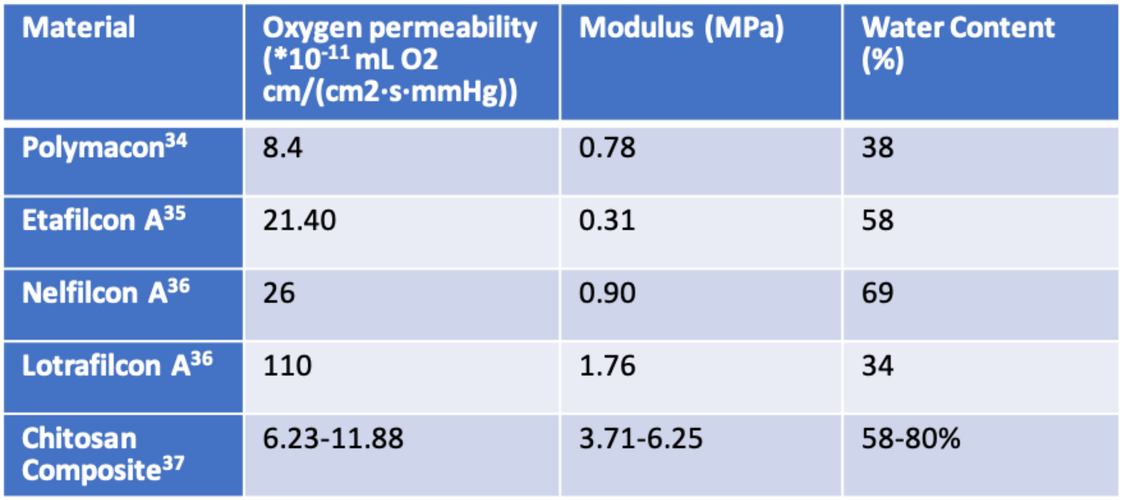

Material	Oxygen permeability (*10^{-11} mL O2 cm/(cm2·s·mmHg))	Modulus (MPa)	Water Content (%)
Polymacon[34]	8.4	0.78	38
Etafilcon A[35]	21.40	0.31	58
Nelfilcon A[36]	26	0.90	69
Lotrafilcon A[36]	110	1.76	34
Chitosan Composite[37]	6.23-11.88	3.71-6.25	58-80%

Table 1: Comparison of common contact lens hydrogel and chitosan composite material. This indicates that chitosan is a potential material for contact lens application.

Chitosan, a co-polymer with alternative units of β-(1 → 4)-D-glucosamine and N-acetyl-D-glucosamine, has been used in biomedical applications due to its biocompatibility and antimicrobial properties.[6] It has been widely researched as a structural component for nanoparticle drug delivery.[6] Shi et al. studied the tensile strength and oxygen permeability of composites containing chitosan and gelatin as contact lens materials.[37] They showed that the modulus of chitosan films is within the range of 3.71-6.25 MPa, which is higher than that in conventional hydrogel contact lenses. They conclude that chitosan has good hydrophilic properties and is a potential biomaterial for contact lens application. (Table 1) In this study, chitosan films are prepared by solvent evaporation and spin casting. Although chitosan is insoluble in water due to its cationic molecules, it still swells in water due to its microporous structures and hydroxyl group interaction with water molecules. In order to control film deformation caused by swelling, the material was crosslinked by chemical or ionic crosslinking agent or both.

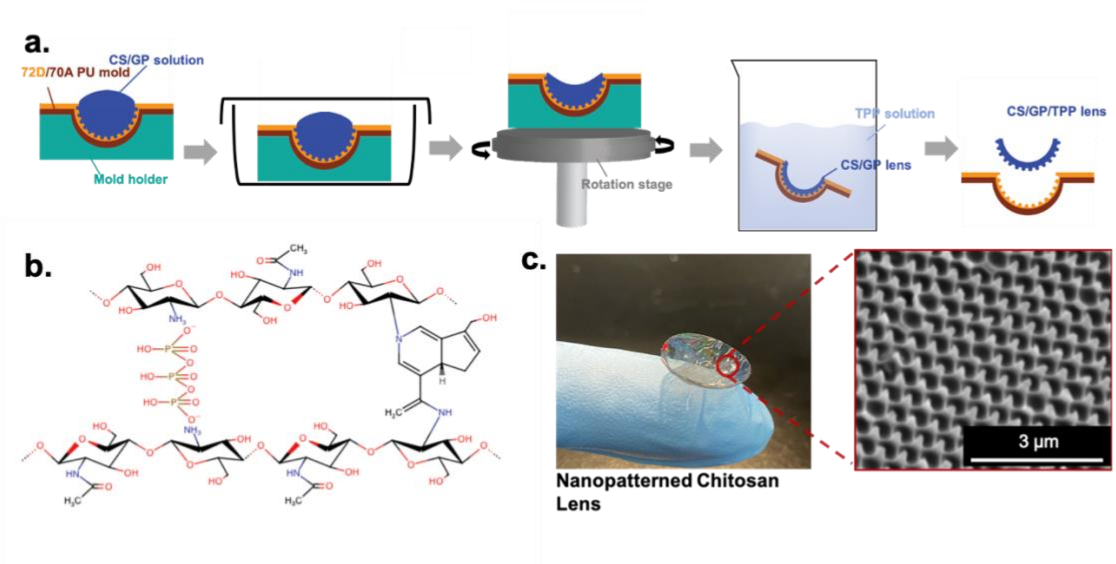

Figure 10: *(a) Schematic of crosslinking process and spin casting for GP/TPP co-crosslinked chitosan lenses. (b) Chemical structure of GP/TPP co-crosslinked chitosan. The amino functional groups either forms covalent bonding with genipin or ionic interaction with TPP molecules. (c) Swollen CS/TPP lenses with nanotopography. The SEM shows the nanopillars that are replicated to the lens.*

To retain geometry and integrity of the contact lens at the swollen state, a dual crosslinking system that consisted of the chemical crosslinker genipin and the ionic crosslinker sodium tripolyphosphate (TPP) was used. Chitosan crystalizes when strong intermolecular hydrogen bonds form between amino and hydroxyl groups.[38] But these hydrogen bonds will break in an acidic environment due to the repulsion between protonated amino groups.[38] Chemical crosslinkers can provides stable and permanent networks to the hydrogel matrix whereas ionic crosslinking provide a higher molecular degree of freedom. Both crosslinkers have been shown to have low toxicity and can be feasible in a physiological environment.[39, 40] The drawback to genipin crosslinked chitosan is the reduction in toughness with increase in modulus.[21] The dual crosslinking system employed in this work is intended for enhancing the material toughness while maintaining the desired modulus for contact lens material. But later in the present study, we show that the single crosslinking system containing only TPP showed a promising result in transparency and stability of lens when swollen. One concern is that TPP crosslinking can be affected by the change of pH in the environment. This is because $P_3O_5^-$ ions from TPP compete with additional OH^- ions to interact with the NH_3^+ protonated amino groups on the chitosan chains.[41] OH^- ions will also deprotonate the amino groups which can potentially hinder the ionic crosslinking. Study shows that pH of conjunctival fluid change from 6.93 to 7.14 when a patient becomes infected with microbial keratitis. This pH change should have little effect on the ionic crosslinking of TPP.

In this chapter, I will characterize both dual and single crosslinking systems and compare the performance of the two systems. The objective of this chapter is to find a crosslinking system with optimal properties for the nanopillared chitosan lens. By investigating the various concentration of chemical and ionic crosslinkers, the optimal concentration of crosslinkers was determined by the lens stability at a swollen state.

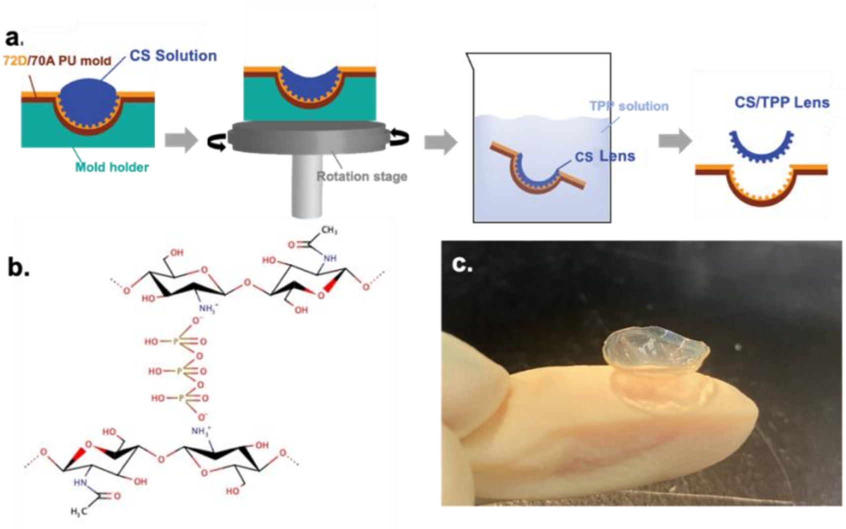

Figure 11: *(a) Schematic of TPP crosslinking process and spin casting of chitosan lenses. (b) Chemical structure of TPP crosslinked chitosan. The amino functional groups form ionic interaction with TPP molecules. (c) Swollen CS/TPP lenses with nanotopography.*

3.2 Experimental Procedure

3.2.1 Crosslinking Methods and Lens Fabrication

3.2.1.1 Prepare chitosan-genipin solution

We adopt in this research a dual crosslinking system with chemical crosslinker and ionic crosslinker. The 2.2 w/v% chitosan solution was prepared by dissolving 90% deacylated chitosan (Qingdao Yunzhou Biochemistry Co.) in 0.1M acetic acid. Genipin(Sigma Aldrich) was dissolved in ethanol to obtain the genipin stock solution. Then the stock solution was added to the chitosan solution to obtain a GP/CS solution with 0.5 mM genipin concentration. The procedure is as follow:

a. Dissolve 0.44 g of chitosan in 20 ml 0.1M acetic acid with stir bar at room temperature to make a 2.2 w/v% chitosan solution.

b. Pre-dissolve genipin in ethanol and calculate the molarity for genipin stock solution:

$$\frac{x\ mg\ of\ genipin}{10mL\ of\ ethanol} = y\ \frac{mg}{mL} = y\ \frac{g}{L} \times \frac{1\ mol}{226.226\ g} = z \times 10^3 mM$$

c. Calculation for making 0.5 mM genipin crosslinked chitosan:

$$0.5\ mM\ \times (V_{genipin\ in\ ethanol} + V_{1.1w/v\%\ chitosan}\ =\ z \times 10^3 mM\ \times V_{genipin\ stock}$$

d. Dissolve $V_{genipin\ stock}$ of genipin stock solution in $(V_{genipin\ in\ ethanol} - V_{genipin\ stock})$ aboslute ethanol, where $V_{genipin\ in\ ethanol}$ is 1/10 of $V_{1.1w/v\%\ chitosan}$.

TPP solution was prepared by dissolving 1 wt%, 2 wt%, and 4 wt% sodium tripolyphosphate (Sigma Aldrich) in Milli-Q water and stir until no visible solute is detectable in the solution.

3.2.1.2 Fabrication of GP/TPP co-crosslinked chitosan lens

GP/CS solution was cast onto the lens-shaped PU negative mold with nanohole structures and covered with a Petri dish for 48 hours for crosslinking. The crosslinked solution was then placed on a rotation stage for spin casting at 110 rpm. The solvent will evaporate at room temperature after 12 hours of spinning at room temperature and the solution eventually becomes a dry film. The centrifugal force acting on the solution helps to form a lens with uniform thickness and to prevent the deformation of the chitosan lens due to volume contraction of hydrogel during the drying process. The dried GP/CS lens was washed with absolute ethanol to remove unreacted genipin and neutralized with 0.1M NaOH to remove residual acid. Then the neutralized lens was immersed in 1%-4% TPP solution for 5 mins for ionic bonds to form between the crosslinker and polymer chains.

After ionic crosslinking, the lens was left to dry at room temperature and peeled off for use after drying. A hole puncher of 14.5 mm in diameter was used to cut the edge of the lens to obtain a smooth margin. This size of the hole puncher can be varied to control the diameter of the lens.

3.2.1.3 Solution preparation for CS/TPP lens

The 2 w/v % chitosan solution was obtained by dissolving 0.4 g of chitosan in 20 ml 0.1M acetic acid and stirring the solution with a stir bar at room temperature until chitosan is fully dissolved. The dissolving process usually takes 12 to 24 hours. A low stirring speed is required to prevent the crystallization of the chitosan in the solution due to chain alignment during the stirring. The 5 wt% and 10 wt% TPP solutions were prepared by adding sodium tripolyphosphate to Milli-Q water and stirring until all sodium tripolyphosphate is dissolved.

3.2.1.4 Fabrication of CS/TPP chitosan lens

A solvent-assisted drop casting method was used to obtain the chitosan lens. 1 ml of the 2 w/v% chitosan solution was cast onto the lens-shaped nanoholed PU mold, which is stabilized on a rotational stage, until the solution covers all edges of the mold. Then the stage was rotated at 110 rpm for overnight to evaporate the solvent and obtain an uncrosslinked chitosan lens. The centrifugal force forms the material into an aspheric base curve where the front curvature is controlled by the curvature of polyurethane mold. The dried chitosan lens on the PU mold was then immersed into 3 ml of 0.1M NaOH for 1 min to neutralize any residual acid in the lens. The lens was then rinsed with Milli-Q water and patted dried with Kimwipe. Then the neutralized chitosan lens on PU mold was directly submerged into 3 ml of 5wt% or 10wt% TPP in Milli-Q water for 1 hour. Afterwards, the chitosan lens was rinsed again with Milli-Q water and patted dry with Kimwipe. The crosslinked chitosan lens was left under room temperature to dry and then peeled off from the mold. Finally, the final lens was punched with a 14.5 mm hole puncher to obtain a smooth lens edge.

3.3 Surface Topography Characterization

Nanopillars on chitosan lens surfaces need to be examined using microscopies with sufficiently high magnification where the few hundreds of nano-scaled features can be imaged. In this study, the scanning electron microscopy (SEM) was used to determine the nanopillar shape and orientation, and atomic force microscopy (AFM) was used to quantitatively measure the pillar heights and diameters. The nanopillars on chitosan lenses with different crosslinking concentrations and post-swelling chitosan lens were characterized. The optimal crosslinking concentration was determined by the uniformity and stability of nanopillars after swelling.

3.3.1 Scanning Electron Microscopy

Pre- and Post-swelled chitosan lenses with different crosslinker concentrations were imaged with the FEI Magellan SEM in the UC Irvine Materials Research Institute (IMRI). Electron beam with low voltage (5 kV) and current (0.2nA) was used to minimize damage to the biopolymer. This is essential when evaluating the nanopillars on chitosan lenses because high energy electron beam will cause deformation of the pillars. All samples were coated with 4nm platinum/palladium (Pt/Pd) using the LEICA sputter coater 200 from in IMRI. The sample stage was tilted by 30 degrees to image the side profile of the nanopillars, which better demonstrate the pillar dimensions and shapes.

The pre-swelled chitosan lenses were fabricated with solvent evaporation and spin casting methods as described in the previous sections. The post-swelled chitosan lenses were first rehydrated in phosphate buffer saline (PBS) for 24 hours, and then lyophilized for a further 24 hours. The cross-section of lyophilized chitosan gel was obtained by freezing the sample with liquid nitrogen and breaking it with tweezers. The air-drying method was also investigated to examine the nanopillars after swelling. The pillar periodicity was measured from the SEM micrographs using the software Image J. The dimensions of nanopillars on the Ni positive mold and its replicated nanostructures on the chitosan lens are compared.

3.3.2 Atomic Force Microscopy

Atomic force microscopy (AFM) was used to assess the heights of nanopillars for each chitosan lens sample. AFM can generate a 3D profile of the nanostructures and quantitatively determine the maxima in heights and curvatures. The AFM images were acquired via the tapping mode at a frequency of ~320 kHz. The silicon AFM tips, purchased from NanoWorld, are aluminum coated for signal enhancement. The cross-sectional profile of nanopillars was exported from Gywddion and graphed with Matlab and R. AFM samples were obtained by cutting out the center area of the lens and kept flat with carbon tapes.

3.4 Materials Properties Characterization

3.4.1 Energy-dispersive X-ray spectroscopy studies

The crosslinked chitosan lenses containing TPP were characterized using energy-dispersive X-ray spectroscopy (EDS), which is an analyzer attachment to FEI Magellan scanning electron microscopy. The energy profile of phosphorus can be used to determine the concentration of ionic crosslinks in the dual crosslinking system. The intensity of phosphorus energy profile will also show if the crosslinking is saturated at a certain crosslinker concentration. The chitosan lens samples were adhered to carbon tape and coated with 5 nm of carbon. The choice of carbon coating is to avoid the overlapping of energy profiles between the coating material and phosphorus. The carbon was coated to the samples using the LEICA sputter coater 200 in IMRI. Energy profiles were scanned at the electron beam voltage of 6 kV and current of 1.6 nA.

3.4.2 Determination of degree of crosslinking

The degree of crosslinking was tested using ninhydrin assay, which uses an agent to bind with free amino groups in the hydrogel. The percentage of crosslinked amino groups can be calculated from the number of free amino groups. The chitosan lens samples were first hydrated for 24 hours and then lyophilized for 24 hours. 3 mg of sample was weighed from each lyophilized sample and reswelled in 10 µL of Milli-Q water to prevent the movement of the sample due to the electrostatic force. Subsequently, 1 ml of ninhydrin reagent (Sigma Aldrich) was added to each sample to react with crosslinked chitosan at 100 °C for 20 min. After the reaction, the ninhydrin solution was diluted with 95% ethanol by 25 folds. The optical absorbance of the diluted solution at 570 nm wavelength was recorded using an Ultraviolet-visible (UV-Vis) spectrophotometer (SpectraMax M3). A standard curve between absorbance and amino group concentration was obtained using glycine solution at various known concentrations. The number of amino groups in chitosan should be proportional to the optical absorbance of reacted ninhydrin solution and can be calculated based on a standard curve. Three samples for each sample group were measured and the average crosslinking degree was taken.

3.4.3 Mechanical Properties

The Young's modulus and yield strength of chitosan with various crosslinker concentrations were evaluated using a tensile tester (TestResource Inc.). 20mm x 2mm testing strips were acquired by cutting flat chitosan films with a hobby knife. To minimize defects on the edge of testing strips, which could weaken the samples and cause an error in measurements, the hobby knife needs to be extra sharp. The testing strip was then clamped between 2 pieces of 1200 grit sandpapers to enhance the friction at the grip and prevent the sample from slipping out during testing. The gage length was controlled at 10 mm for all samples. The testing strip was pulled by the top grip at a rate of 0.5 mm/s until the sample breakage. Measurement was only taken when the sample strip breaks at the center. Five measurements were made for each sample and the average value is obtained. The film thickness was measured for each sample by imaging the cross-section with an optical microscope and analyze the thickness via Image J software. The strain and stress were calculated from the recorded force and elongation.

3.4.4 Transparency

The ability of crosslinked chitosan films and lenses to transmit light was measured using a UV-vis spectrometer over the visible light spectrum, where the wavelength range from 200 to 800 nm. We investigated the transmittance of hydrogel with different combinations of crosslinker concentrations and different topography. Commercially available HEMA based contact lenses (Biotrue ONEday, Bausch+Lomb) were set as the control group where the HEMA lens has no coloration and is optically transparent. The chitosan samples were swollen for 24 hours in PBS to reach an equilibrium state before measuring their transparency. The samples were cut into a circular shape with 6mm diameter discs and fitted into the wells on the 96 well plate. 200 μL of

PBS was added to each well to prevent the sample from drying. The average transmittance over a range of wavelength is calculated by:

$$T_{avg} = \frac{\sum_{400nm}^{800nm} T_\lambda \times \Delta_\lambda}{\sum_{400nm}^{800nm} \Delta_\lambda}$$

Where the T_{avg} is the average transmittance over a wavelength range of 400nm to 800nm; T_λ is the transmittance at a certain wavelength, and Δ_λ is the difference between two wavelengths.

3.4.6 Swelling Behavior

To investigate the stability of the crosslinked chitosan lens, the water content of the lens over 7 days was measured. By investigating the various concentration of covalent (GP) and ionic (TPP) crosslinkers, the optimal concentration of crosslinkers was determined by the lens stability at a swollen state. A hydrogel contact lens with high water content will allow more oxygen to reach the cornea through the water in between the porous networks. Conventional hydrogel contact lenses obtain water content range from 38% to 70%;[29] therefore our chitosan lens is aiming to maintain a water content of ~ 100%.

The dimensions of pre-swollen samples were constrained to have a base curve radius of 8.4 mm and a diameter of 14.5 mm to fit the eyes of New Zealand white rabbits. Three samples for each sample group were immersed in 10 ml PBS separately and left in an incubator shaker at 34°C to simulate the physiological environment in the cornea surface. The swelling ratio and water content was calculated with the equation below:

$$\text{Swelling Ratio (\%)} = \left(\frac{W_f - W_i}{W_i}\right) \times 100$$

$$\text{Water Content (\%)} = \left(\frac{W_f - W_i}{W_f}\right) \times 100$$

where W_f is the weight of lens after a time interval *t*, Wi is the initial weight of lens measure when the lens is still dry.

3.4.7 Fourier-transfer infrared spectroscopy

The co-crosslinked chitosan lenses with chemical crosslinker concentrations of 0.5 mM and ionic crosslinker concentrations of 1%,2%, and 4% are characterized by Fourier-transfer infrared spectroscopy (FTIR, Nexus 670). All spectra were recorded in the range of 600 - 4000 cm^{-1}. The sample was folded twice to increase the scanned volume and fit between the sample stage the IR probe.

3.5 Result and Discussion

3.5.1 Scanning Electron Microscopy characterization

3.5.1.1 Concentration of chitosan solution

The concentration of polymers in its solution is related to its viscosity. At higher concentrations, polymer chains may interpenetrate or align with their surrounding chains and form chain entanglements. On the other hand, polymer chains in dilute solutions have less interaction with their surrounding chains.[42] For successful nanofabrication, particularly of nanopillars, a critical concentration is needed. A solution with too low of concentration will not have enough material to form dense polymer networks to support nanopillars, and too high of concentration also will not result in self-assembled nanopillars due to the great shear stress at the wall of nanoholes. Two concentrations, 1.5 wt% and 2 wt%, of chitosan solution were tested in this study. These two concentrations result in dry films with acceptable thickness in the range of 100-200 um, which is determined by the commercial contact lenses. A solution with lower concentration is expected to form taller pillars due to the lower viscosity. The SEM images (Figure 12) show that 1.5 wt% solution forms taller nanopillars, but these pillars collapsed during demolding. By comparison the 2 wt% chitosan solutions formed uniform nanopillars from the solvent evaporation process. These nanopillars are found to be strong enough to maintain their pillar shape after demolding. Thus, 2 wt% is a proper concentration for nanopillar fabrication on the chitosan film. The thickness of chitosan films can be tuned by alternating the volume of chitosan solution.

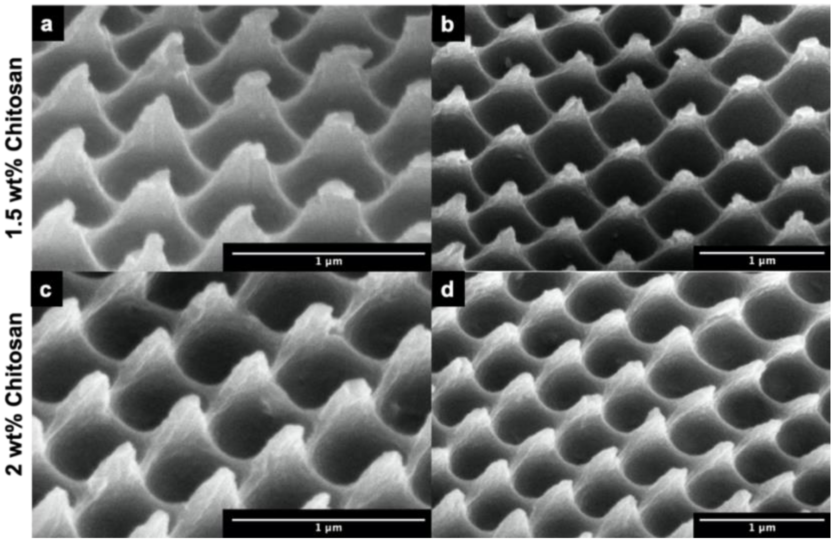

Figure 12: Nanopillared surface on chitosan lenses made from 1.5wt% and 2wt% chitosan solution. Scale bar =1 μm.

3.5.1.2 GP/TPP Co-crosslinked Chitosan Lens

To make the resulting lens stable at a swollen state, the chitosan lens was crosslinked with both covalent and ionic crosslinkers. The concentration of genipin is chosen based on findings from previous student, where a 0.5mM is sufficient for forming nanopillars easily. The topography of chitosan lenses crosslinked with 0.5mM genipin and 0%, 1%, 2%, or 4% TPP are characterized at the pre-swelling state. The crosslinking process was separated into two steps where the genipin chemical crosslinking is the first step. The hypothesis is that the shape and dimension of the nanopillars would be determined by the first step in the crosslinking process. TPP should only diffuse into the film to crosslink the remaining free amino groups with little effect on the geometry of nanopillars. The SEM images in Figure 13 show that the nanopillars on all four lenses with different concentration combinations form uniform arrays without any collapsing. These replicated nanopillars appear to be the accurate reproductions of the Ni positive mold in terms of the pillar diameter and periodicity. These micrographs also indicate that the solvent-assisted drop casting lithography can produce consistent nanostructures.

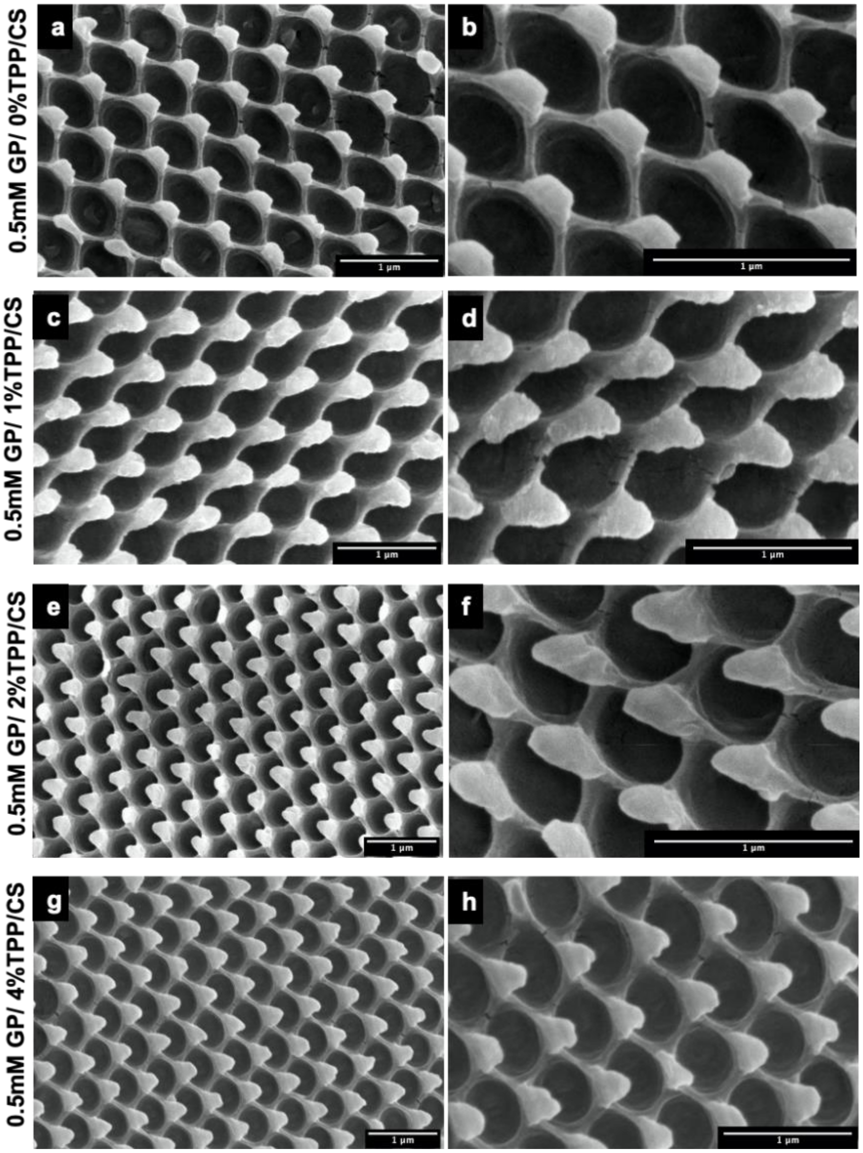

Figure 13: Representative SEM images of nanopillared surface of GP/TPP co-crosslinked chitosan lenses with crosslinker concentration of 0.5mMGP/0%TPP (a,b), 0.5mMGP/1%TPP (c,d), 0.5mMGP/2%TPP (e,f), 0.5mMGP/4%TPP (g,h). *Scale bar =1 µm.*

The aspect ratio and density of the nanopillars will influence the efficiency of the antimicrobial effect.[3, 21] We choose to investigate the post-swelling pillar morphology of 0.5mM GP/ 1% TPP and 0.25mM GP/ 2% TPP due to their appropriate swelling ratio (shown in section 3.5.3) as a contact lens material. The topography before and after swelling is characterized with SEM. The volume contraction of air-dried CS/TPP lenses results in nanopillar shrinkage shown in

Figure 14. Lyophilized CS/TPP lenses are able to maintain the geometry of nanopillars but result in hydrogel brittleness and breakage of nanopillars. The SEM micrographs (Figure 14) show that the swollen films maintain nanoscale patterns that are results of pillar shrinkage. To further explore the actual nanopillar geometry on the chitosan surface at the hydrated state, we lyophilized the swollen chitosan lens to look at their topography. Lyophilization allows the frozen solvent to sublimate and escape from the chitosan hydrogel films while sustaining the geometry of the hydrogel matrix. Volume expansion of solvent due to crystal forming may result in freeze thawing of the hydrogel matrix. Figure 15 shows that the nanopillars on lyophilized 0.5mM GP/1% TPP/CS lenses are deformed and the pillar periodicity have expanded due to swelling, which demonstrates that the nanopillars are not stable with this co-crosslinking system. The surface of 0.25mM GP/ 2% TPP/CS lens only shows a porous structure, similarly to the cross-section morphology. The lower chemical crosslinking concentration leads to larger hydrogel networks which allow more solvent to diffuse into the hydrogel. The hydrogel morphology is therefore strongly dependent on the first step of crosslinking which is the chemical crosslinking. Thus, we can conclude that neither 0.5mM GP/ 2% TPP/CS nor 0.25mM GP/ 2% TPP/CS lenses are suitable for this application due to the unstable surface nanostructure that result from these compositions.

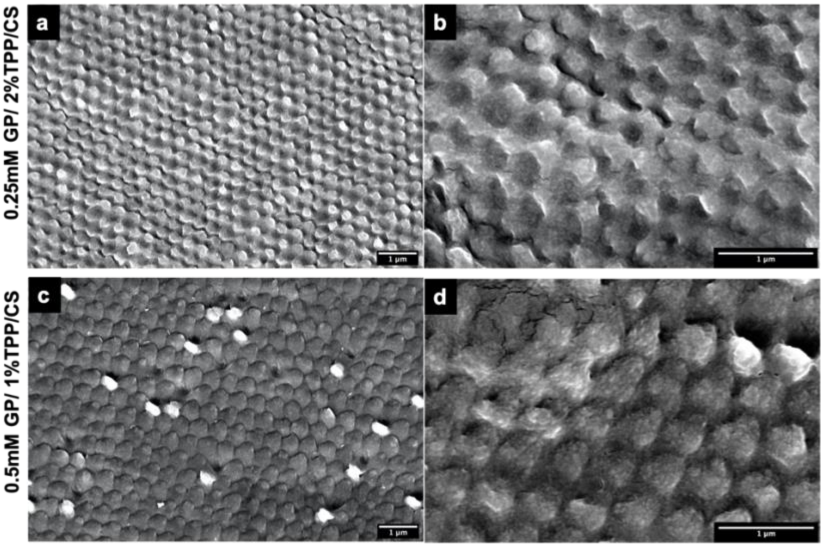

Figure 14: SEM micrographs of air-dried GP/TPP co-crosslinked chitosan lenses. Scale bar =1 μm.

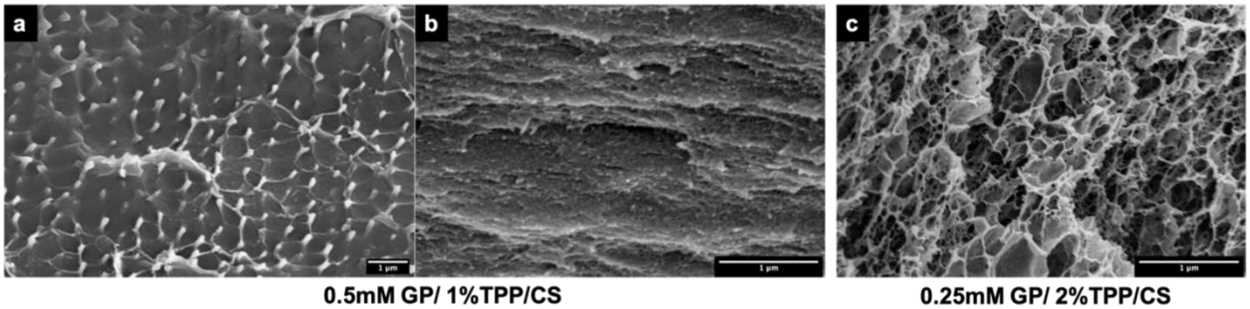

Figure 15: *SEM micrographs of lyophilized GP/TPP co-crosslinked chitosan lenses. (b) and (c) are the cross-sections of the chitosan hydrogel lenses. Scale bar =1 μm.*

3.5.1.3 TPP Crosslinked Chitosan Lens

Representative SEM micrographs of nanopillars on chitosan films crosslinked by TPP show that they exhibit stable and uniform morphologies at the pre-swelling stage. Chitosan films with no crosslinking also formed uniform arrays of nanopillars with few collapses observed due to demolding. By contrast, the flat chitosan surface showed that the ionic crosslinking has little effect on the morphology of the surface. Both 5% TPP and 10% TPP crosslinked chitosan lenses obtain nanopillars with high aspect ratios. The pillar periodicity of CS/TPP lenses is maintained at 500 nm, which is the same as the that of nanopillars on the Ni positive mold.

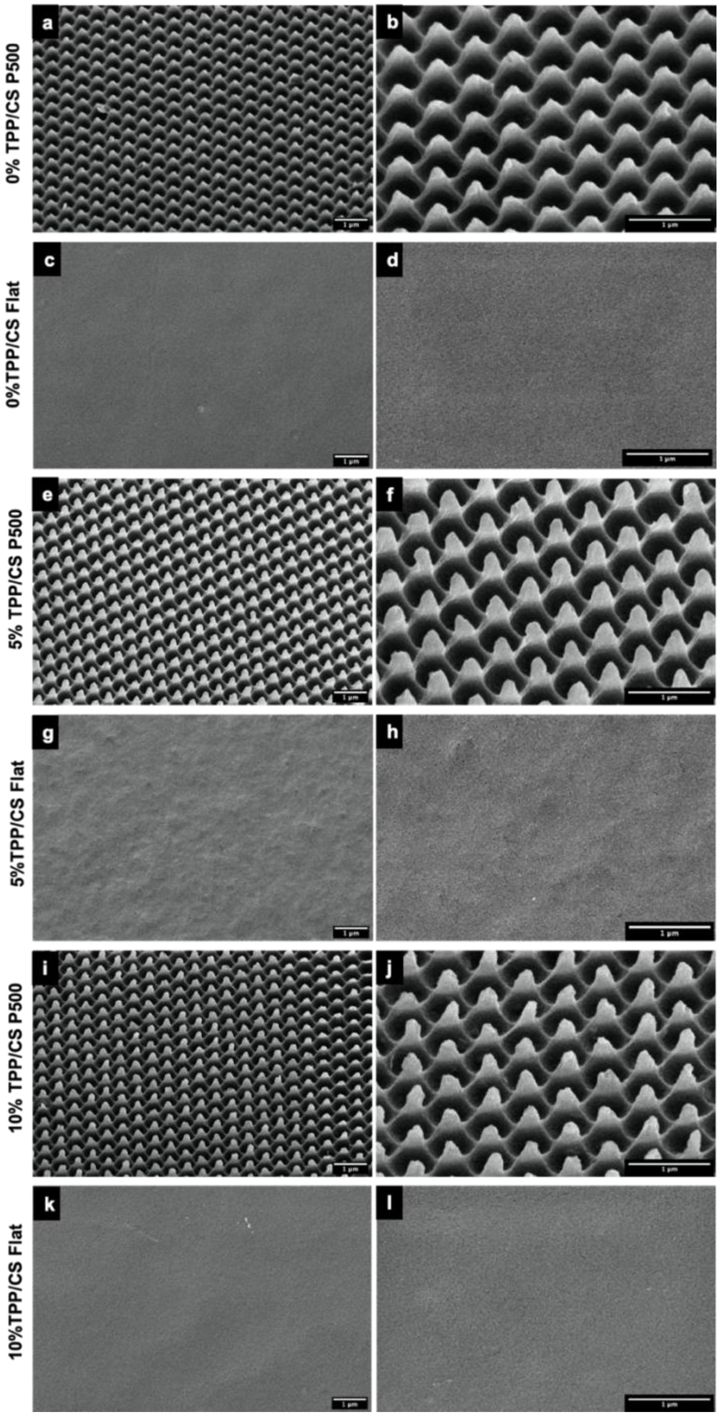

Figure 16: SEM images of CS/TPP P500 lenses and flat films before swelling with TPP concentration of 0% (a,b,c,d), 5%(e,f,g,h) and 10% (i, j, k,l). Scale bar =1 µm.

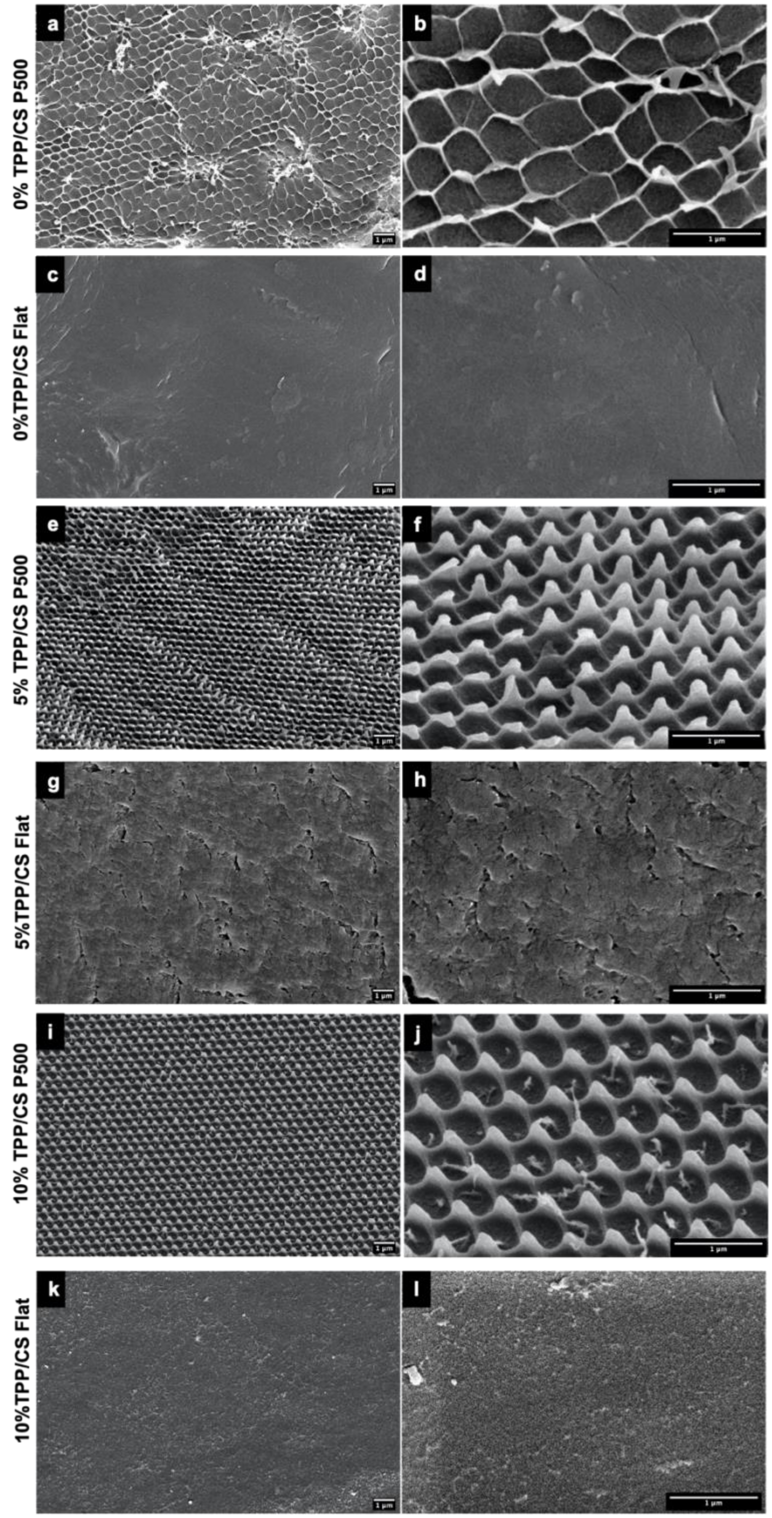

Figure 17: *The films are swelled to reach an equilibrium state. SEM images of lyophilized CS/TPP P500 lenses and flat films with TPP concentration of 0% (a,b,c,d), 5%(e,f,g,h) and 10% (i, j, k,l). Scale bar =1 µm.*

Lyophilized lenses were imaged with SEM to determine the stability of nanopillars at the post-swelling state. All lenses were swollen for 24 hours to reach the equilibrium state. The chitosan lens with no crosslinker exhibits the most pillar deformation due to volume expansion as expected. (Figure 17) The amino and hydroxyl groups on chitosan chains are not fixed by crosslinker and therefore can interact with the water molecules, which results in the large volume expansion and unstable matrix structure. In comparison, the 5% TPP crosslinked chitosan lens still maintained the nanopillar geometry after swelling with few defects observed. The best pillar stability is shown on the 10% TPP crosslinked chitosan lenses, as the pillars are still maintained in arrays with no deformation. There are some nanoscale impurities observed on lenses and flat film surfaces which might be a result of contaminated PBS. Figure 17 proves that the chitosan lenses crosslinked with 10% TPP have the ideal pillar geometry and stability in the hydrated state.

3.5.2 Atomic Force Microscopy characterization

3.5.2.1 GP/TPP Co-crosslinked Chitosan Lens

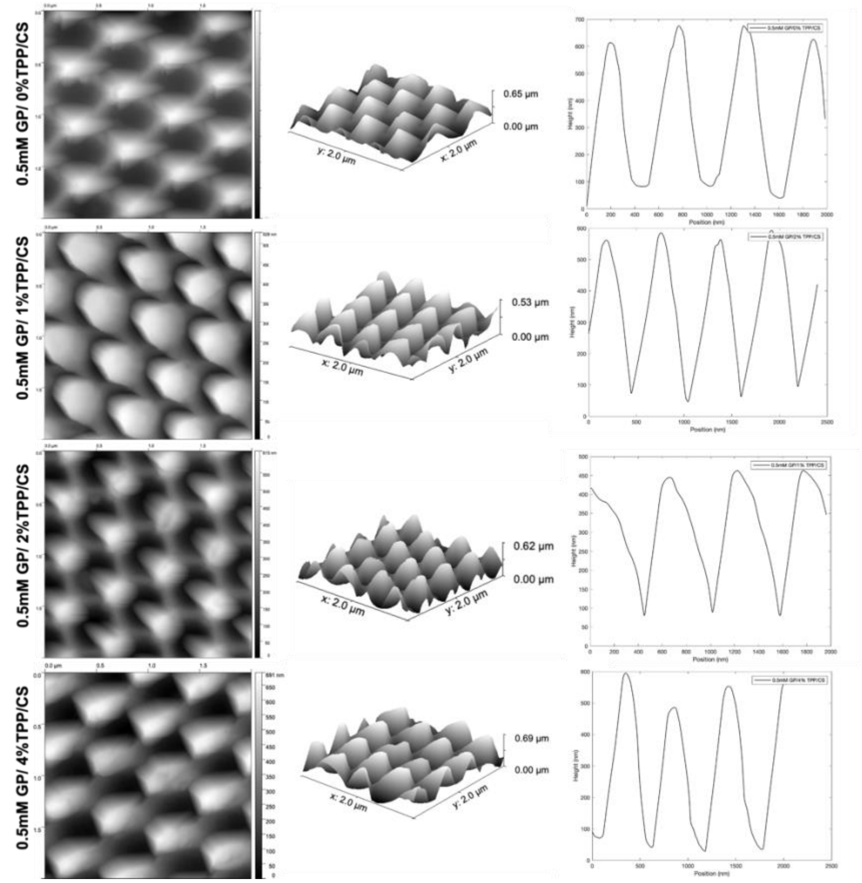

Figure 18: AFM scans, 3D profiles and cross section profiles of GP/TPP/CS P500 lenses and flat films before swelling with crosslinker concentration of 0.5mMGP/0%TPP, 0.5mMGP/1%TPP, 0.5mMGP/2%TPP and 0.5mMGP/4%TPP.

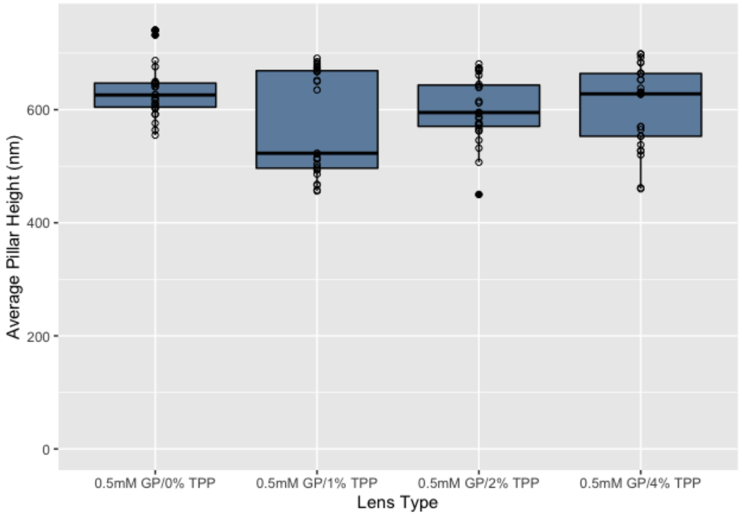

Figure 19: The average pillar heights of GP/TPP co-crosslinked chitosan lenses with crosslinker concentration of 0.5mMGP/0%TPP, 0.5mMGP/1%TPP, 0.5mMGP/2%TPP, 0.5mMGP/4%TPP. 10 pillars were analyzed from each film (n=2).

The heights of nanopillars are characterized using AFM. Figure 18 shows 3D profile and cross-section profile of the nanopillars on chitosan lenses co-crosslinked by 0.5mM genipin and 0%, 1%, 2% or 4% TPP. The average heights are summarized in the bar graph in Figure 19. The average pillar height of 0.5 mM/0% TPP and 0.5 mM/4% TPP are similar. Each experiment group only contains heights measurements from 2 lenses. The 0.5 mM/ 1% TPP has the lowest average pillar height which might be due to the outliers. The result will be more accurate with larger sample groups.

3.5.2.2 TPP Crosslinked Chitosan Lens

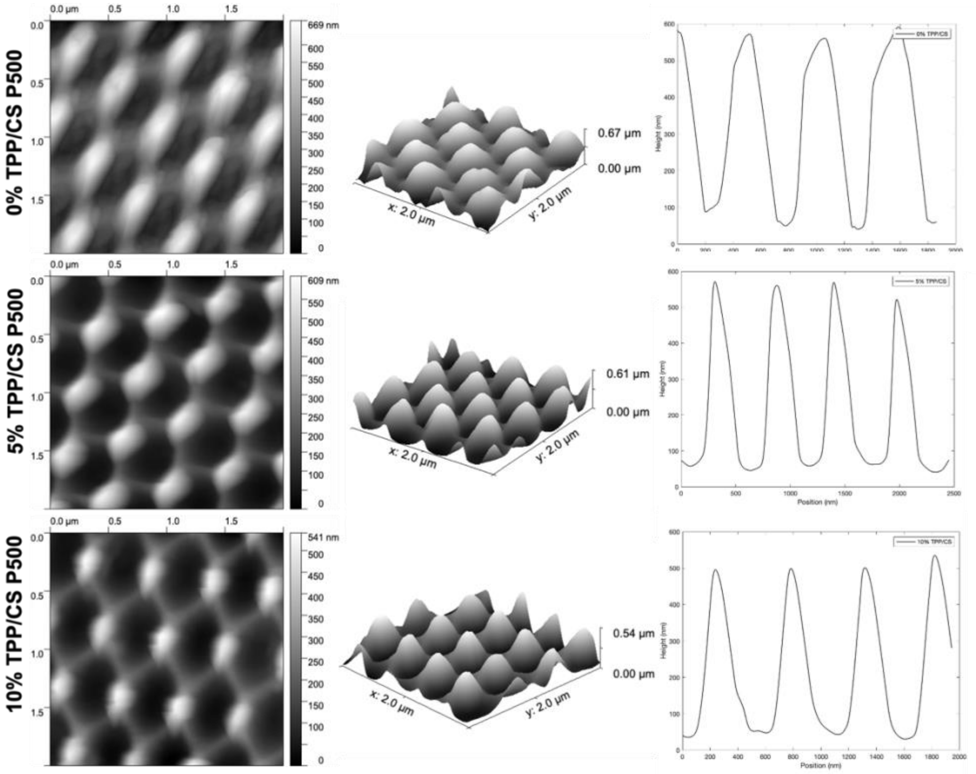

Figure 20: AFM scans, 3D profiles, and cross section profiles of TPP/CS P500 lenses and flat films before swelling with TPP concentration of 0%TPP, 5%TPP, and 10%TPP.

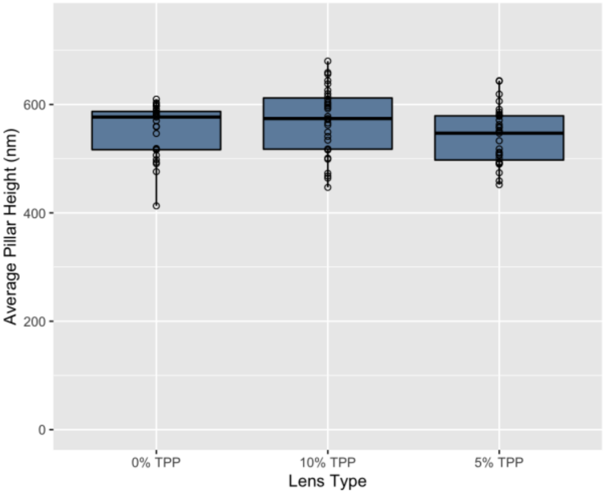

Figure 21: The average pillar heights of TPP crosslinked chitosan lenses with crosslinker concentration of 0%TPP, 5%TPP, and 10%TPP. 10 pillars were analyzed from each film (n=3).

The average pillar heights of nanopillars on 0% TPP, 5% TPP, and 10% TPP chitosan lenses are similar to the nanohole depth of PU negative lens mold. This validates that the solvent assistant drop-casting nanolithography is an appropriate method for replicating nanopillars to chitosan hydrogel. There is no significant difference in pillar heights between chitosan lenses crosslinked with different TPP concentrations. This demonstrates that the ionic crosslinker does not affect the morphology of nanotpography using the immersion crosslinking method.

3.5.3 Swelling Behavior

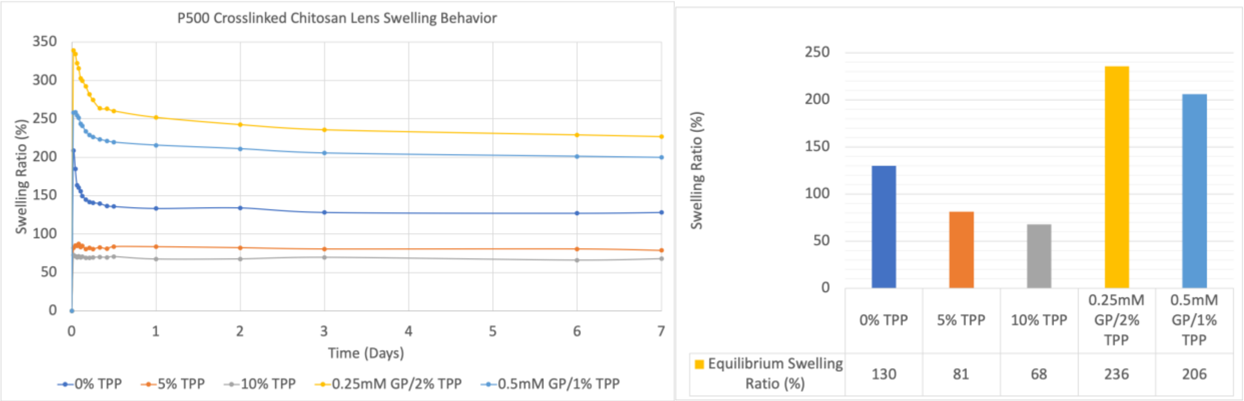

Figure 22: The swelling ratios of 0% TPP, 5% TPP, 10%TPP, 0.25mM GP/2%TPP and 0.5mM GP/1% TPP chitosan films. The equilibrium swelling ratio of GP/TPP crosslinked films is significantly higher than TPP crosslinked films. All films contain P500 nanotopography. (n=3)

To examine the dynamic swelling behavior of crosslinked chitosan lenses, the lenses were swelled in PBS for 7 days. Mechanistically, the higher degree of crosslinking will result in reduced pore size of hydrogel networks, therefore, decrease the swelling ratio. The swelling behavior of crosslinked chitosan demonstrates that GP/TPP co-crosslinked chitosan lenses have a higher equilibrium swelling ratio compared to the non-crosslinked and TPP crosslinked chitosan lenses. (Figure 22) The high swelling ratio of GP/TPP co-crosslinked chitosan causes distortion of the lens at a hydrated state and decreased stability of lens geometry. The chemical crosslinking of genipin happens while polymer chains are still suspended in the solvent. These observations could be because, while the genipin prevents chitosan networks from forming crystalline regions, whereas the non-crosslinked chitosan chains can rearrange into the crystalline region during the solvent evaporation process. If this is true then genipin crosslinked networks should be more amorphous, which would cause the increase in water content. The equilibrium swelling ratio of TPP crosslinked chitosan lenses are within the proper range for contact lens material. The large fluctuation in swelling ratio can increase internal stress in material, which lead to deformation of nanopillars. Unlike the co-crosslinked chitosan lenses, the single crosslinked chitosan lenses have no large fluctuation in swelling ratio before reaching equilibrium swelling, which indicates that the single crosslinking system is optimal for maintaining the lens geometry at swollen state.

3.5.4 EDS studies

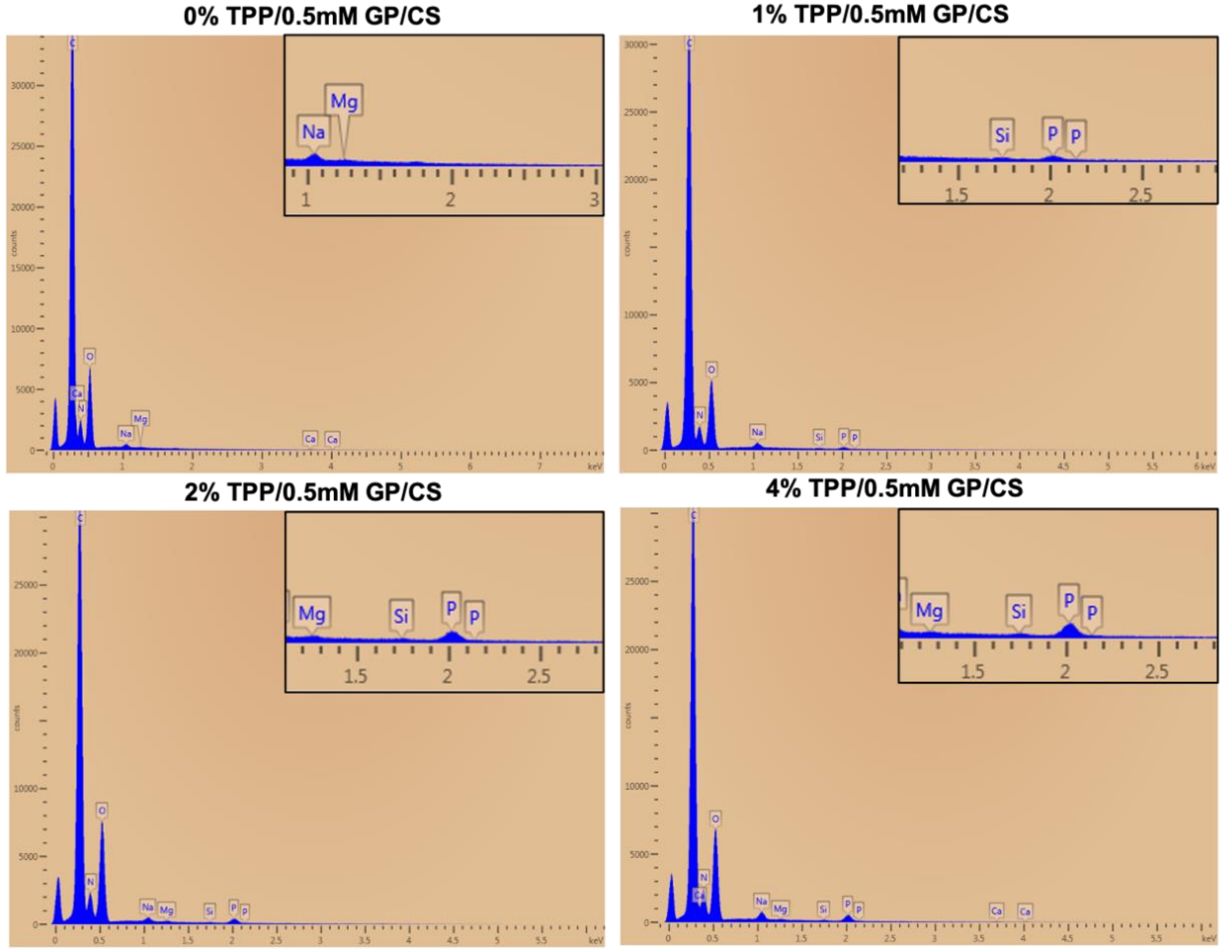
0% TPP/0.5mM GP/CS

1% TPP/0.5mM GP/CS

2% TPP/0.5mM GP/CS

4% TPP/0.5mM GP/CS

Figure 23: EDS energy profiles of GP/TPP co-crosslinked chitosan lenses with crosslinker concentration of 0.5mMGP/0%TPP, 0.5mMGP/1%TPP, 0.5mMGP/2%TPP and 0.5mMGP/4%TPP. The Kα peak for phosphorus is identified at 2.02 keV.

Element	0% TPP (Wt%)	1% TPP (Wt%)	2% TPP (Wt%)	4% TPP (Wt%)
N	30.93	26.39	24.43	28.48
O	64.11	64.26	64.98	55.92
Na	2.48	4.30	2.44	4.37
Mg	0.42	0	0.64	0.43
Ca	2.07	0	0	1.81.57
Si	0	1.02	0.48	0.76
P	0	4.04	7.02	8.47

Table 2: The elemental analysis of GP/TPP co-crosslinked chitosan lenses with crosslinker concentration of 0.5mMGP/0%TPP, 0.5mMGP/1%TPP, 0.5mMGP/2%TPP and 0.5mMGP/4%TPP.

The energy profile of phosphorous distributed on the nanopillared surface of co-crosslinked chitosan lenses is examined by EDS to evaluate the relative amount of ionic crosslinking. Chitosan lenses crosslinked with genipin shows no trace of phosphorous. The elemental analysis shows that the ionic crosslinking increased as the concentration of TPP increased without reaching the saturation in crosslinking. This observation demonstrates that the free NH_3^+ groups in the GP/CS lenses can still be fixed by ionic crosslinking. TPP can penetrate the chitosan matrix to form ionic bonds with the protonated amino groups. The degree of crosslinking also demonstrates the same tendency. The mass percentage of phosphorous for 5%TPP and 10%TPP crosslinked chitosan lenses are higher than the GP/TPP co-crosslinked lenses, which is expected as the concentration of crosslinker increases. The data shows the 5% TPP crosslinked chitosan is not at the saturation point in crosslinking.

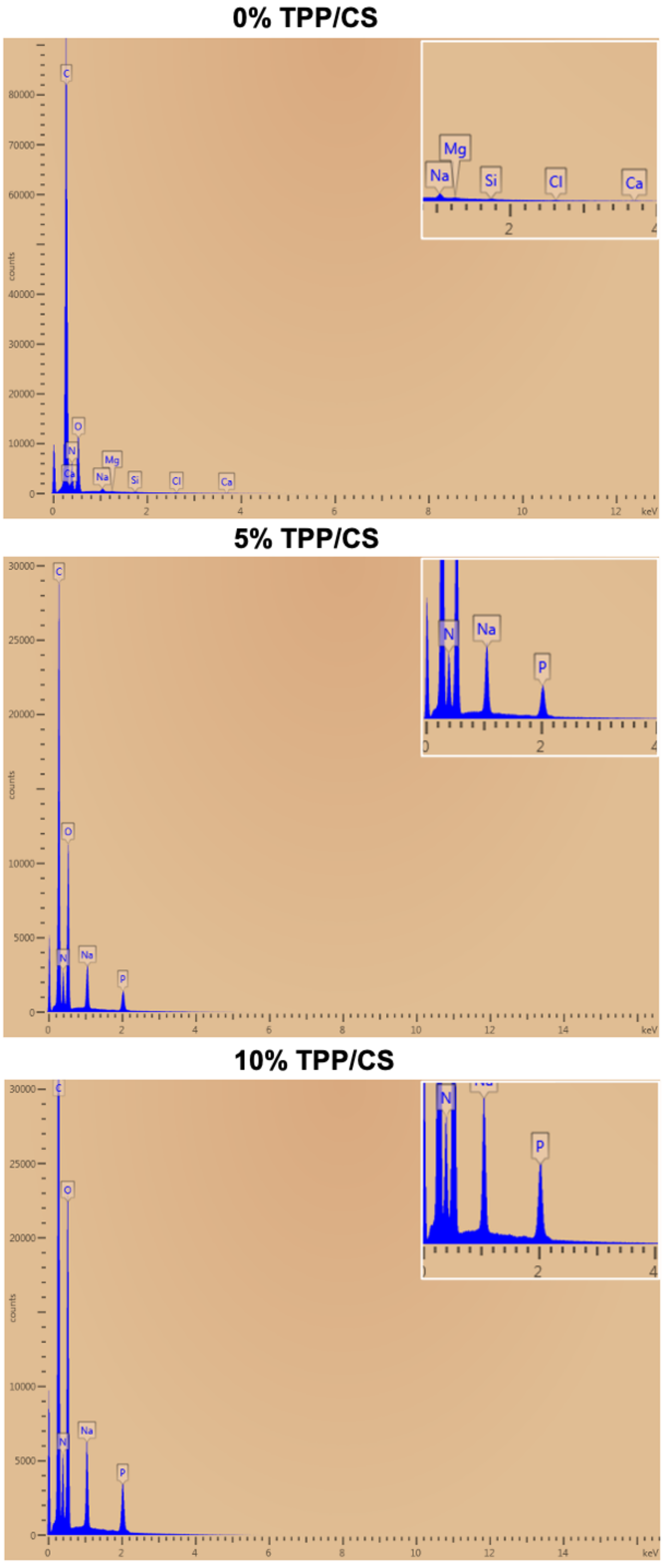

0% TPP/CS

5% TPP/CS

10% TPP/CS

Figure 24: EDS energy profiles of TPP crosslinked chitosan lenses with crosslinker concentration of 0%TPP, 5%TPP, and 10%TPP. The intensity of phosphorus Kα peak indicates the amount of P in the chitosan film.

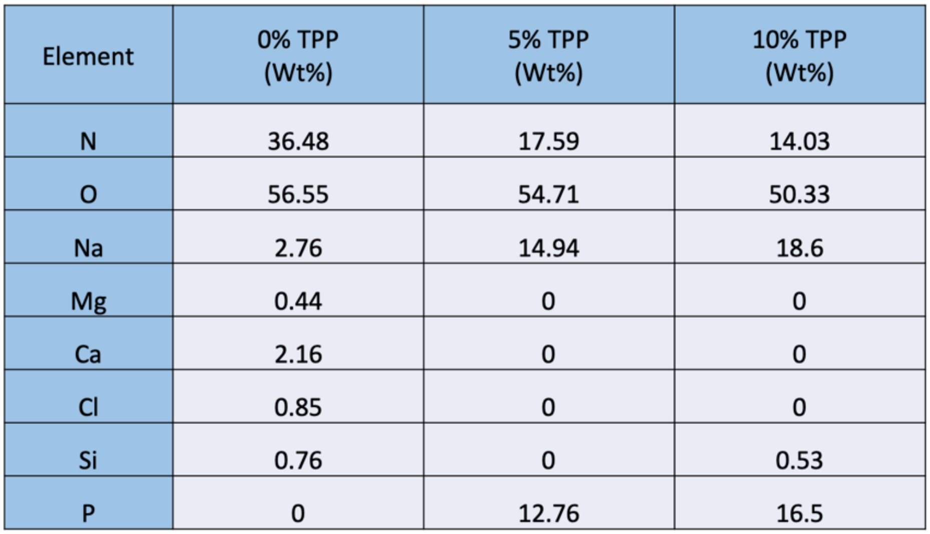

Element	0% TPP (Wt%)	5% TPP (Wt%)	10% TPP (Wt%)
N	36.48	17.59	14.03
O	56.55	54.71	50.33
Na	2.76	14.94	18.6
Mg	0.44	0	0
Ca	2.16	0	0
Cl	0.85	0	0
Si	0.76	0	0.53
P	0	12.76	16.5

Table 3: The elemental analysis of TPP crosslinked chitosan lenses with crosslinker concentration of 0%TPP, 5%TPP, and 10%TPP.

3.5.5 Ninhydrin Assay

Swelling behavior data demonstrate that the GP/TPP co-crosslinked chitosan lenses had a much higher swelling ratio than the TPP single crosslinking system. This indicates that the GP/TPP chitosan networks have lower crosslinking density than the single crosslinking system, which is also verified by the degree of crosslinking (DoC) data shown in Table 3. The surface morphology of lyophilized GP/TPP co-crosslinked chitosan shows a large volume expansion of the matrix, which also demonstrates that GP/TPP co-crosslinked chitosan has a lower crosslinking density. The degree of crosslinking increases by two orders of magnitude as the concentration of TPP crosslinker doubles.

Lens Type (P500)	Average DoC (%)
0.5 mM GP/1% TPP/CS	14
0.5 mM GP/2% TPP/CS	24
0.5 mM GP/4% TPP/CS	41

Table 4: The degree of crosslinking data of GP/TPP co-crosslinked chitosan P500 lenses with crosslinker concentration of 0.5mMGP/1%TPP, 0.5mMGP/2%TPP and 0.5mMGP/4%TPP. (n=3)

The degrees of crosslinking of TPP crosslinked flat films and P500 lenses were also evaluated. The data suggest that the presence of nanostructures on the hydrogel surface apparently increases the degree of crosslinking of the chitosan films. Heedy et al. also observed that the confinement of nanostructure can promote the alignment of the polymer chains.[21] The intermolecular interaction between chains is enhanced during the nanofabrication process. Even for chitosan matrix with no crosslinker, the affiliation of nanostructure increases the degree of crosslinking from 35% to 65%, which is a result of enlargement of the crystalline region due to chain alignment.

Film Type	Average DoC (%)
0% TPP/CS Flat	35
5% TPP/CS Flat	75
10% TPP/CS Flat	67
0% TPP/CS P500 Lens	65
5% TPP/CS P500 Lens	79
10% TPP/CS P500 Lens	84

Table 5: The degree of crosslinking data of TPP crosslinked chitosan lenses and flat films with crosslinker concentration of 0%TPP, 5%TPP, and 10%TPP. (n=3)

3.5.6 Tensile Properties

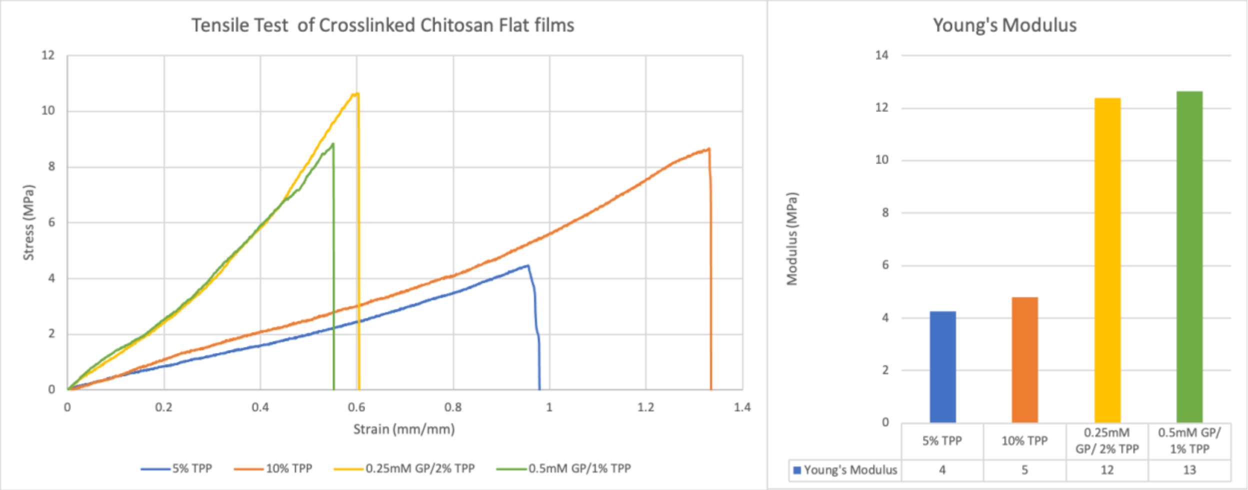

Figure 25: The representative stress/strain curves of 5% TPP, 10%TPP, 0.25mM GP/2%TPP and 0.5mM GP/1% TPP chitosan flat films. Young's modulus is calculated from the slope of the linear region on the curves. (n=5)

The modulus of the hydrogel is an important factor for determining the comfort of the contact lens. It is believed that it will also affect the durability of contact lenses. Commercial contact lenses usually obtain a range of modulus around 0.4 – 1.5 MPa. Tensile behavior of the GP/TPP co-crosslinked chitosan are compared with the TPP single crosslinked chitosan flat films. (Figure 25) The modulus of co-crosslinked films is found to be significantly higher than single crosslinked films while the fracture strains are much lower. Thus, higher modulus and lower fracture strain correspond to the higher crosslinking density of the dual-crosslinking hydrogel films. Yet, according to the ninhydrin test, the crosslinking degree of the dual crosslinking systems is much lower than the single crosslinking system. The fact that GP/TPP co-crosslinked chitosan films have higher tensile modulus might be due to the higher bond dissociation energy of covalent bonds. It was observed in this study that the single crosslinking system is able to prevent lens from changing shape for 7 days.

3.5.7 Transparency studies

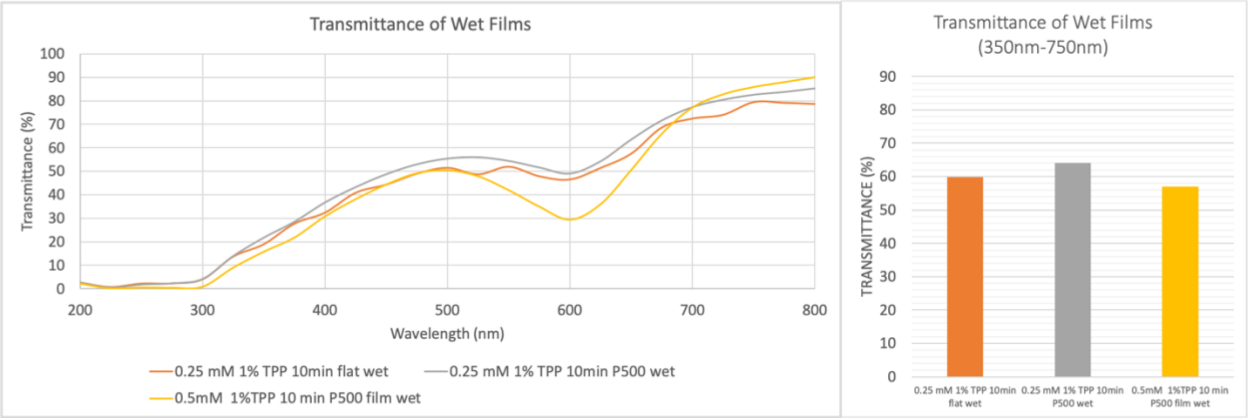

Figure 26: Transmittance of wet co-crosslinked chitosan films in the visible light spectrum. The nanotopogtaphy has little effect on the transmittance of the crosslinked films when the film is hydrated. (n=3)

The light transmittance of 0.5 mM GP samples was observed to be lower than the 0.25 mM and 0 mM GP samples for both films and lenses. As the concentration of genipin increases, the absorption of 600 nm light (orange) by the crosslinked chitosan films increases which renders a blue coloration. The nanostructures on the surface of the chitosan lens have little effect on the light transmittance when transmittance is measured normal to the film plane, shown in Figure 26. Overall, all co-crosslinked chitosan lenses have a degree of transparency ranging from 57%-67% in the visible light spectrum (400nm-800nm). It is known that UV radiation from the sun can damage the cornea and slow down the cornea's healing process. The co-crosslinked chitosan lenses have the potential to protect the injured eye from UV exposure. These lenses obtain optical transmittance of 17%-25% in the UV waveband (200nm-400nm), which indicates medium to high reduction of sun glare and good UV protection.

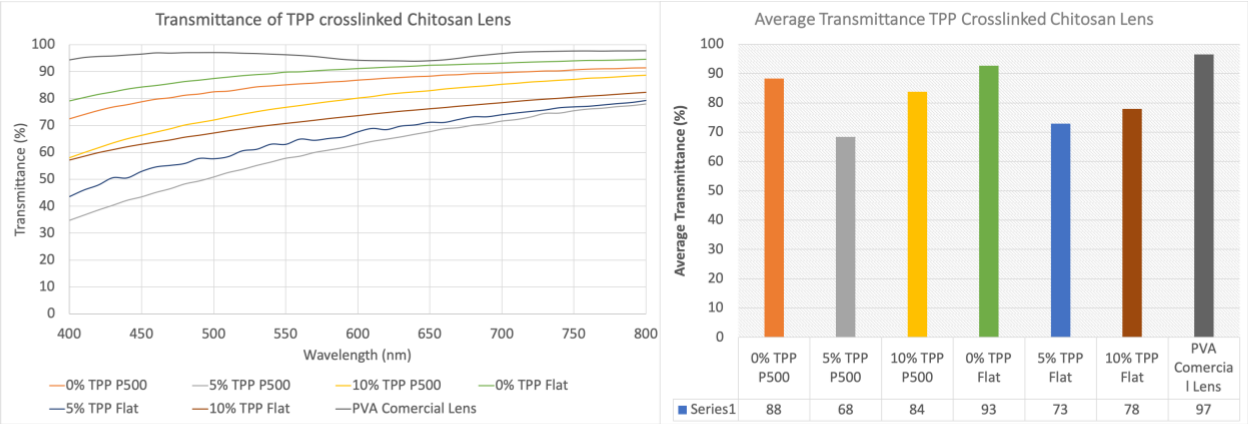

Figure 27: Optical Properties of flat and nanopillared TPP crosslinked chitosan lenses over the visible light spectrum. The average transmittance of CS/TPP lenses are compared to the HEMA based commercial contact lenses. The nanotopogtaphy has little effect on the transmittance of the crosslinked films when the film is hydrated. (n=3)

The GP/TPP co-crosslinked chitosan lens is reported to have an average transmittance of 57%-67% in the visible light spectrum (400nm-800nm). This range is not within the acceptable transmittance range for commercially available contact lenses. The low transmittance is due to the crosslinking mechanism of genipin which renders a blue coloration as the crosslinked film absorbs light with a wavelength ~600nm. Genipin reacts with amino groups from chitosan to form heterocyclic amines under an acetic environment and produces a dark blue coloration.[43] With increased TPP concentration from 1% to 5% and 10%, the crosslinked chitosan lens can maintain the aspherical shape without the presence of covalent crosslinking due to genipin. The average transmittance of TPP single crosslinked chitosan lens can reach 84% in the visible light spectrum (Figure 27). We hypothesize that the increase in transparency from 5% TPP/CS lenses to 10% TPP/CS lenses may be due to the reduction in the size of the crystalline region, and therefore scatter less at the boundary between crystalline and amorphous regions. This can be examined by Small Angle X-ray Scattering (SAXS) in the future work. We conclude that 10% TPP crosslinked P500 chitosan lenses shows the best transparency.

3.5.8 FTIR studies

The co-crosslinked chitosan lenses with different concentrations of ionic crosslinking were characterized by Fourier-transform infrared spectroscopy (FTIR). The electrostatic interaction between negatively charged TPP and positively charged amino groups on chitosan should be detectable in terms of shifts in intensities or absorption bands in the IR spectrum. Specifically, the P=O bond is the characteristic bond for the presence of TPP in the crosslinked films. Therefore, the intensity of P=O stretching peak can be used to determine the amount of TPP that is obtained in the chitosan lens.

The infrared spectrum of chitosan showed characteristic saccharide structure peaks for C-O stretching at 1024 and 1064 cm^{-1}, and antisymmetric stretching of C-O-C bridge at 1152 cm^{-1}.[44] The protonated amide group is shown around 1550 cm^{-1}. The appearance of a strong peak at 1640 cm^{-1} can be assigned to C=O stretching in the amide group. Several authors have posited that the evidence of ionic crosslinking is the new band that forms at 1203 cm^{-1} assigned to the antisymmetric stretching vibration of the PO_2 group in TPP ions. But there are no significant peaks can be around 1203 cm^{-1}. This might be due to the shifting of the peak due to antisymmetric movement.

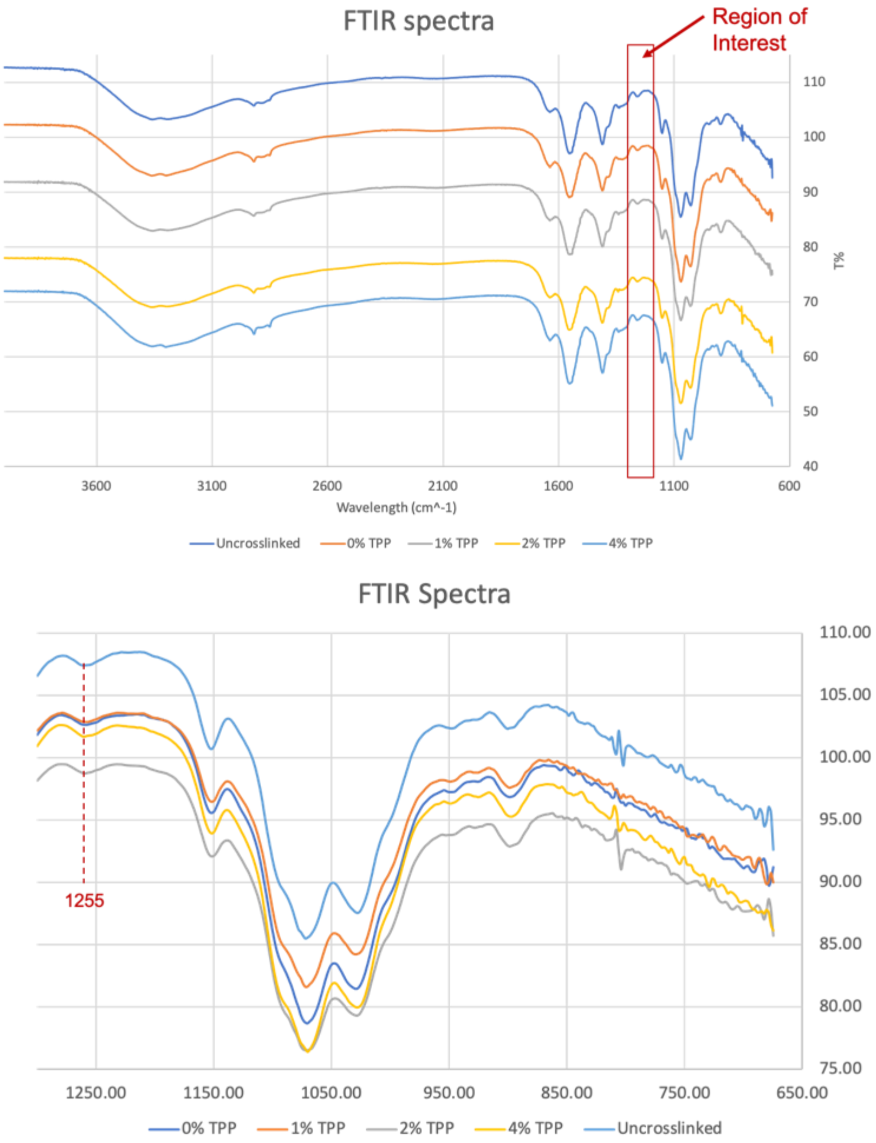

Figure 28: FTIR spectra of CS/GP/TPP lens prepared with different TPP concentrations. The bottom graph is an expansion of the region of interest. The P=O stretching peak is not detected in this region.

Chapter 4: In vitro Antifungal Study of Nanopatterned Contact Lens

4.1 Objective

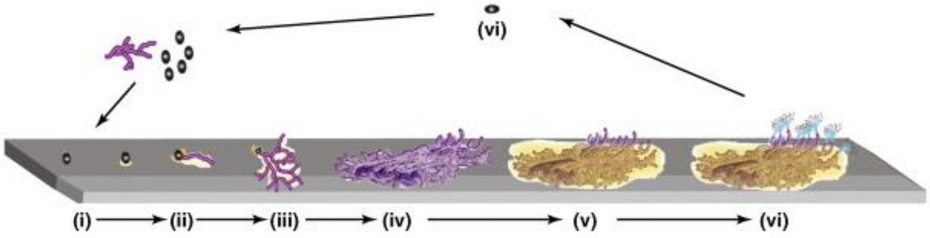

Figure 29[45]: Schematic of biofilm development in filamentous fungi. The process includes the following stages: (i) adsorption of fungi and their spores, (ii) active attachment and sporulation, (iii) formation of microcolony I, (iv) formation of microcolony II, (v) development of the mature biofilm, and (vi) planktonic phase. This figure is modified from Harding et al.

Fungal adhesion is the initial step for fungal growth and biofilm formation, which can decrease the susceptibility of fungi to chemical antifungal methods. The fungal cell wall is a composition of polysaccharide β-1,6-glucan, chitin, and cell wall proteins.[46] Some of the cell wall proteins have intracellular functions and can influence cell metabolism. The stress applied from the nanopillars to the cell wall could interference with the normal cell function and therefore inhibit cell attachment and growth.[2] To examine the antifungal efficacy, we established an in vitro fungal adhesion assay where the fungus spores are suspended in the nutrient media and can settle onto the testing surface.[47] The adherent cells are cultured for an extended period of time and quantified microscopically at time intervals. To accurately characterize if the antifungal activity arises from the presence of nanopillars instead of from the release of material components, control groups of flat surfaces made with the same material are also cultured under the same condition. Fungal growth on polystyrene and polydimethylsiloxane (PDMS) are also recorded as the negative control as these surfaces are known to be nonresistant to fungus.[48] It is known that surface hydrophobicity varies between different materials and will influence the adhesive properties of fungi.[49]

Filamentous fungus like *Fusarium oxysporum* is a common soilborne pathogen that is invasive to humans.[50] Fungal spores release adhesin to attach to a surface and germinate into hyphal fragments in nutrient culture media. (Figure 29) A microcolony of fungus will then produce extracellular matrix to form biofilm. The hyphal elongates and branches within the biofilm and releases hyphae fragments as spores for a new cycle of growth.[43] The hyphae networks do not only grow parallel to the host surface but also perpendicular to the surface in the form of layers. (Figure 29) Once the three-dimensional networks are formed, they can limit the observation of the bottom fungi layer adhesion. In order to solve this problem, floating non-adherent organisms must be flushed away before imaging.

Fusarium oxysporum is engineered to include green fluorescing protein (GFP) gene which is used to monitor the fungal growth under the florescence microscope. The GFP will be activated with blue light and emit green fluoresce. The fluorescence images can provide structural information of the fungi, and the intensity of GFP can be used to quantify the fungal mass in an in vitro environment. In this study, the attachment and growth of *F. oxysporum* on various surfaces are characterized, and the change of fungal mass over time is concluded.

4.2 Experimental Procedures

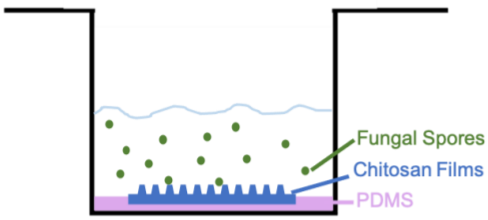

Figure 30: Schematic of in vitro study sample set up. P500 and flat chitosan films are adhered onto the polystyrene well plate using PDMS.

In vitro antifungal study on nanopillared (P500) and flat chitosan films crosslinked with 5%TPP and 10%TPP was performed to evaluate the antifungal efficacy of a nanopillared chitosan surface. A GFP expressing strain of *Fusarium oxysporum* (GFP 8996) was used in the study. The *Fusarium oxysporum* spores were collected from the matured *Fusarium oxysporum* hyphae networks on the Sabouraud Dextrose (SD) agar plate and filtered using cotton gauze. Spores were swelled in SD broth for 5 hours to develop initial germinations before plating them on sample surfaces.

The dry CS/TPP films were cut into 16 mm diameter circular-shaped specimens and adhered to the bottom of polystyrene well (d = 22 mm) using PDMS. (Figure 30) PDMS was cured for 48 hours at room temperature to fix CS/TPP films in the well plates. Then the CS/TPP films were swelled in culture media RPMI 1640 (Gibco Inc.) for 24 hours before experiments to reach an equilibrium swollen state.

Fusarium oxysporum spores were plated on triplicated surfaces of each pattern at a concentration of 1×10^5 spores/film. The samples were incubated in 2 ml of fungal growth media (RPMI 1640) containing initial spore count of $5*10^4$/ml at 34 °C with stirring at 100 rpm. The green fluorescent protein images were taken at 0 hr, 2 hrs, 4 hrs, 8 hrs, 16 hrs, and 24 hrs with 10X magnification lens on the fluorescence microscope (Cytation 5 Imaging Multi-Mode Reader). After 24 hours of incubation, the samples were fixed with 10% formalin(Sigma Aldrich) for 15 minutes and dehydrated with a serial dilution of ethanol. The dehydrated films were then sputter coated with 4 nm platinum and imaged with SEM.

4.3 Result and Discussion

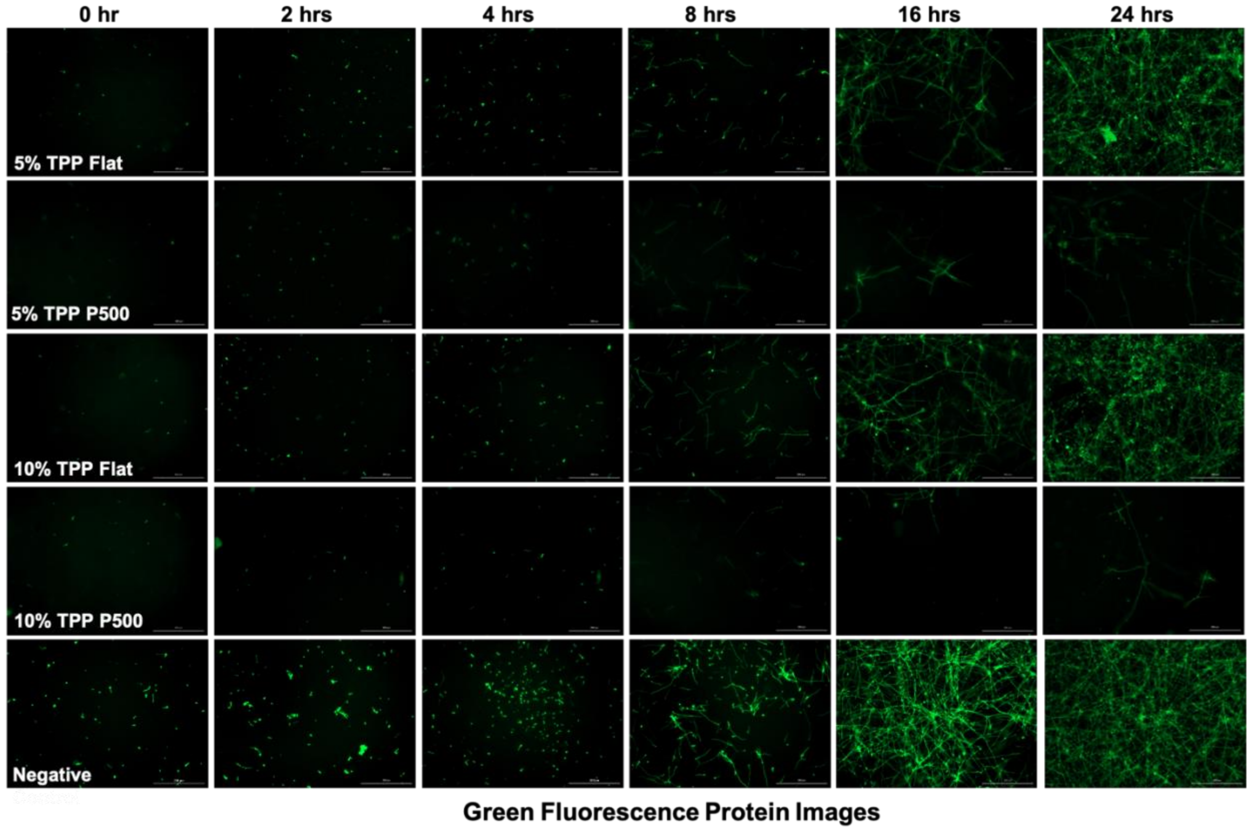

Figure 31: Green fluorescent protein images of F. oxysporum growth on flat and P500 chitosan films crosslinked with TPP concentration of 5%TPP and 10% TPP after 2 hrs, 4hrs, 8 hrs, 16hrs, and 24 hrs of incubation. (n=3) Scale bar = 200µm.

The GFP fluorescence images in Figure 31 show that most germ tubes had developed on the flat surfaces and negative control surfaces after 4 hours of incubation. In comparison, germ tubes were inhibited on the P500 surfaces at the 4 hours point. Nanopillared surfaces have fewer hyphae growth after 8 hours of incubation. The antifungal effect of nanopillared surface lasted for 24 hours. The 10% TPP crosslinked chitosan P500 films have the greatest fungal growth inhibition. (Figure 31) The negative control surface and flat chitosan films are completely covered with hyphae and biofilm after 24 hours of incubation. The fungal mass will be determined by the amount of fluorescence from the images. Detachment of germ rubes from the nanopillared surface was observed after 8 hours of incubation. (Figure 31) Thus, the nanopillars can not only prevent the fungal adhesion but also limit the cyclic hyphal spore secretion behavior.

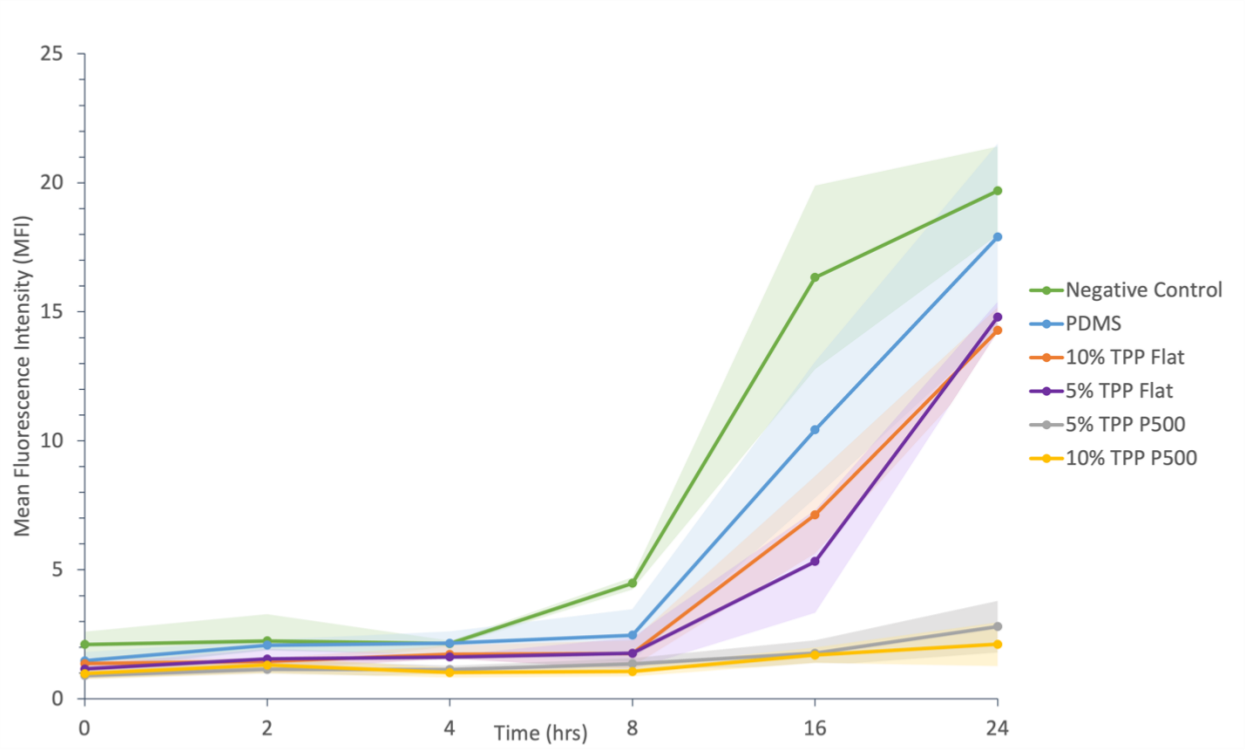

Figure 32: The fungal mass on flat and P500 TPP/CS surfaces are analyzed at each time interval for 24 hours.

Among all the surfaces, 10% TPP/CS P500 surface has the best antifungal effect. The flat TPP/CS surfaces have similar results in fungal growth, which indicates that the concentration of crosslinker does not affect the antifungal properties of the material. (Figure 32) As an antimicrobial material, chitosan surfaces have lower fungal growth than negative control polystyrene surfaces. 5% TPP/CS and 10% TPP/CS P500 surfaces have similar fungal control ability for the first 16 hours.

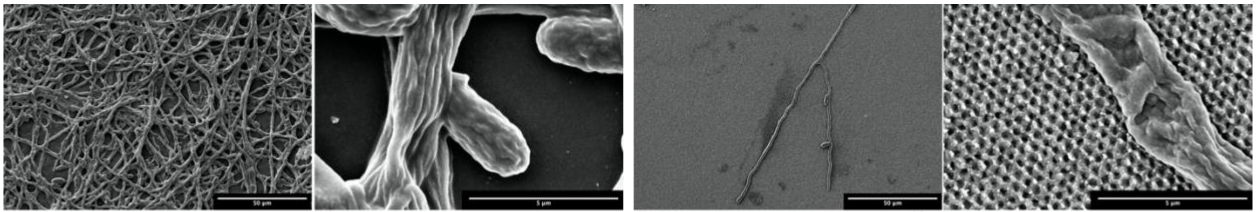

5% TPP Flat

5% TPP P500

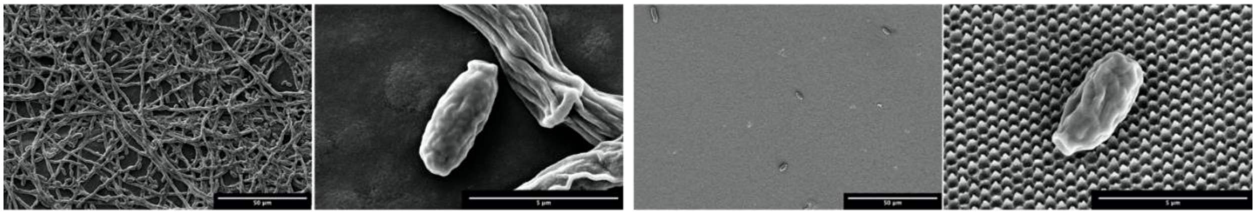

10% TPP Flat

10% TPP P500

Figure 33: Representative SEM images of Fusarium oxysporum on P500 chitosan films crosslinked with TPP concentration of 5%TPP and 10% TPP after 24hrs of incubation. (Scale bar = 50 µm for image with low magnification; scale bar = 5 µm for image with high magnification.)

The interaction between surface topography and fungi cell are analyzed using scanning electron microscopy (SEM). (Figure 33) The ellipsoidal cells observed in the micrograph are the *F. oxysporum* spores. Spores on the flat surface exhibit spherical shape, whereas the spores and hyphae on nanopillared surfaces were found to be deflated. The low magnification image shows that pillared surfaces have limited hyphae growth compared to the flat surface, which is covered with layers of hyphae. Fungi cells can shrink due to the dehydration and fixation process, but deflation was observed with flattened cell walls. Consequently, these observations are not caused by artefacts in specimen preparation. In conclusion, the study has demonstrated the antifungal properties of pillared TPP/CS surfaces and their potential in the application of contact lens design.

Chapter 5: Future Outlooks

In this study, the transparency data of TPP crosslinked chitosan hydrogel shows an increase in opacity when the samples are crosslinked with 5%TPP and a decrease when the crosslinker concentration increases to 10%. It is known that the opacity of polymers results from light diffraction at the boundary between the amorphous and crystalline regions or microdomains. Light can only pass through the material when the regions are too small to interference with light. The transparency data indicates that the 5% TPP crosslinked chitosan films have a larger phase region. Both the swelling behavior and ninhydrin test data shows that the nanopillared films have a higher degree of crosslinking than flat films. These findings lead to a question: how will nanostructures affect the material crystallinity and crosslinking mechanism at the nano scale? The size of the crystalline region and degree of crystallinity can be examined by small angle X-ray scattering (SAXS). We can also use thermoanalytical techniques to analyze the amount of crystalline in the materials. Differential scanning calorimetry (DSC) can measure the amount of energy required to melt or decompose the material. In theory, materials with higher crystallinity need more heat to separate the crystalline regions.

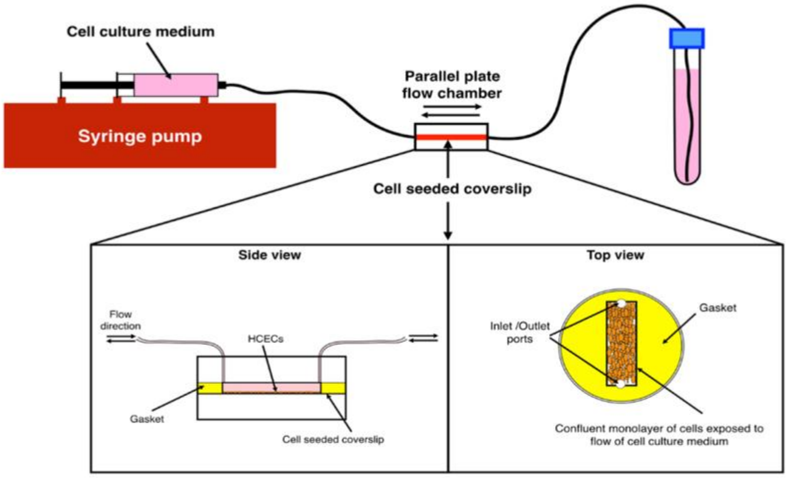

Figure 34[51]: An example of microfluidic system used in in vitro study.

When a contact lens is introduced to the eye, tear films are divided into two sections: pre- and post-lens tear films. The two sections are thinned from the primary tear film, which could result in increase of friction between the contact lens and cornea. Tear film is formed from three layers: a lipid layer, an aqueous layer, and a mucin layer. The lipid layer has with an average thickness of 42 nm and prevents the underlying aqueous phase from evaporating.[52] The aqueous layer is mostly a salt solution and forms 90% of the tear film volume. The mucin layer consists of glycoproteins coated on the surface of the cornea, and acts as an adhesion layer between the aqueous layer and the cornea. During a blink, the stability of the tear film is disturbed by spreading new tear flow from the lacrimal gland. The lipid layer contains non-polar and polar molecules (Figure 2), where the polar layer phase separates from the aqueous layer immediately following the blink and forms a stratified flow. The *in vitro* study can be modulated to mimic the physiological environment for microbes in certain conditions. For instance, the microbes that cause keratitis will experience the shear stress from tear and eyelid during blinking. Instead of a steady microbe culture, we can incorporate a flow system (Figure 34) to mimic the flow of tear at the surface of contact lens. Unlike in a static culture, non-adherent microorganisms will be flushed away during the experiments. The flow system can be achieved by using microfluidic channels.

REFERENCE

1. Shijie He, Yewang Su, Baohua Ji, Huajian Gao, Some basic questions on mechanosensing in cell–substrate interaction, Journal of the Mechanics and Physics of Solids, Volume 70, 2014, Pages 116-135, ISSN 0022-5096, https://doi.org/10.1016/j.jmps.2014.05.016.
2. Kristian Kolind, Alireza Dolatshahi-Pirouz, Jette Lovmand, Finn Skou Pedersen, Morten Foss, Flemming Besenbacher, A combinatorial screening of human fibroblast responses on micro-structured surfaces, Biomaterials, Volume 31, Issue 35, 2010, Pages 9182-9191, ISSN 0142-9612, https://doi.org/10.1016/j.biomaterials.2010.08.048.
3. Rosenzweig, R., Marshall, M., Parivar, A., Ly, V. K., Pearlman, E., & Yee, A. F. (2019). Biomimetic Nanopillared Surfaces Inhibit Drug Resistant Filamentous Fungal Growth. ACS Applied Bio Materials, 2(8), 3159–3163. https://doi.org/10.1021/acsabm.9b00290
4. Bandara CD, Singh S, Afara IO, Wolff A, Tesfamichael T, Ostrikov K, Oloyede A. Bactericidal effects of natural nanotopography of dragonfly wing on Escherichia coli. ACS Appl Mater Interfaces. 2017;9:6746–60.
5. Jaggessar, A., Shahali, H., Mathew, A., & Yarlagadda, P. K. (2017). Bio-mimicking nano and micro-structured surface fabrication for antibacterial properties in medical implants. *Journal of Nanobiotechnology*, *15*(1). https://doi.org/10.1186/s12951-017-0306-1
6. Landriscina, A., Rosen, J., & Friedman, A. J. (2015). Biodegradable chitosan nanoparticles in drug delivery for infectious disease. *Nanomedicine*, *10*(10), 1609–1619. https://doi.org/10.2217/nnm.15.7
7. Mingxian Liu, Huanjun Zheng, Juan Chen, Shuangli Li, Jianfang Huang, Changren Zhou, Chitosan-chitin nanocrystal composite scaffolds for tissue engineering, Carbohydrate Polymers, Volume 152, 2016, Pages 832-840, ISSN 0144-8617, https://doi.org/10.1016/j.carbpol.2016.07.042.
8. Austin, A., Lietman, T., & Rose-Nussbaumer, J. (2017). Update on the Management of Infectious Keratitis. *Ophthalmology, 124*(11), 1678–1689. https://doi.org/10.1016/j.ophtha.2017.05.012
9. Montes M, Chayet AS, Castellanos A, Robledo N. Use of bandage contact lenses after laser in situ keratomileusis. J Refract Surg 1997; 13(5 Suppl):S430-1.
10. Stapleton, F., Carnt, N. Contact lens-related microbial keratitis: how have epidemiology and genetics helped us with pathogenesis and prophylaxis. Eye 26, 185–193 (2012). https://doi.org/10.1038/eye.2011.288
11. Mauger TF, Hill RM. Corneal epithelial healing under contact lenses. Quantitative analysis in the rabbit. Acta Ophthalmol (Copenh). 1992 Jun;70(3):361-5. doi: 10.1111/j.1755-3768.1992.tb08580.x. PMID: 1636399.
12. Gromacki, S., D., O., S., M., & O., F. A. A. (2012). The Case for Bandage Soft Contact Lenses. Review of Cornea and Contact Lenses. Retrieved from https://www.reviewofcontactlenses.com/article/the-case-for-bandage-soft-contact-lenses
13. Williams, R. L., Levis, H. J., Lace, R., Doherty, K. G., Kennedy, S. M., & Kearns, V. R. (2019). Biomaterials in Ophthalmology (Vol. 1). Encyclopedia of Biomedical
14. Montgomery ML, Fuller KK. Experimental Models for Fungal Keratitis: An Overview of Principles and Protocols. Cells. 2020 Jul 16;9(7):1713. doi: 10.3390/cells9071713. PMID: 32708830; PMCID: PMC7408389.

15. Kernien, J. F., Snarr, B. D., Sheppard, D. C., & Nett, J. E. (2018). The Interface between Fungal Biofilms and Innate Immunity. *Frontiers in Immunology*, *8*. https://doi.org/10.3389/fimmu.2017.01968
16. Xiaoyan Zhang, Xuguang Sun, Zhiqun Wang, Yang Zhang, Wenbo Hou; Keratitis-Associated Fungi Form Biofilms with Reduced Antifungal Drug Susceptibility. *Invest. Ophthalmol. Vis. Sci.* 2012;53(12):7774-7778. doi: https://doi.org/10.1167/iovs.12-10810.
17. Jenkins, J., Mantell, J., Neal, C., Gholinia, A., Verkade, P., Nobbs, A. H., & Su, B. (2020). Antibacterial effects of nanopillar surfaces are mediated by cell impedance, penetration and induction of oxidative stress. *Nature Communications*, *11*(1). https://doi.org/10.1038/s41467-020-15471-x
18. Pogodin, S. et al. Biophysical model of bacterial cell interactions with nanopatterned cicada wing surfaces. Biophys. J. 104, 835–840 (2013).
19. W. F. Coombs and H. A. Knoll "Spincasting Contact Lenses," Optical Engineering 15(4), 154332 (1 August 1976). https://doi.org/10.1117/12.7971986
20. Eyenirvaan Follow. (n.d.). *Manufacturing methods of soft contact lens - presentation at www.eyen...* SlideShare. https://www.slideshare.net/Eyenirvaan/manufacturing-methods-of-soft-contact-lens.
21. Heedy, S., Marshall, M. E., Pineda, J. J., Pearlman, E., & Yee, A. F. (2020). Synergistic Antimicrobial Activity of a Nanopillar Surface on a Chitosan Hydrogel. *ACS Applied Bio Materials*, *3*(11), 8040–8048. https://doi.org/10.1021/acsabm.0c01110
22. Tian, Q., Takács, E., Krakovský, I., Horváth, Z., Rosta, L., & Almásy, L. (2015). Study on the Microstructure of Polyester Polyurethane Irradiated in Air and Water. *Polymers*, *7*(9), 1755–1766. doi: 10.3390/polym7091481
23. Avitabile, G., Picone, D., Merlino, A., Maglio, G., & Caruso, U. (n.d.). Polyurethanes. http://www.whatischemistry.unina.it/en/maglpolyuretan.html.
24. Lu, G., Kalyon, D.M., Yilgör, I. and Yilgör, E. (2003), Rheology and extrusion of medical-grade thermoplastic polyurethane. Polym Eng Sci, 43: 1863-1877. https://doi.org/10.1002/pen.10158
25. Koberstein, J. T., & Galambos, A. F. (1992). Multiple melting in segmented polyurethane block copolymers. *Macromolecules*, *25*(21), 5618–5624. https://doi.org/10.1021/ma00047a010
26. Vu, Lien & Chen, Chao-Chang & Yu, Chia-Wei. (2018). Optical design of soft multifocal contact lens with uniform optical power in center-distance zone with optimized NURBS. Optics Express. 26. 3544. 10.1364/OE.26.003544.
27. Chew, A. C., Chan, A., Nongpiur, M. E., Peh, G., Barathi, V. A., Lwin, N. C., Ong, C., & Perera, S. (2017). A Rabbit Model Study to Determine the Efficacy of a Prototype Corneal Endothelium Protector during Cataract Surgery. *Journal of Ophthalmology*, *2017*, 1–7. https://doi.org/10.1155/2017/6906139
28. Hemadevi Boomiraj, Vidyarani Mohankumar, Prajna Lalitha, Bharanidharan Devarajan; Human Corneal MicroRNA Expression Profile in Fungal Keratitis. *Invest. Ophthalmol. Vis. Sci.* 2015;56(13):7939-7946. doi: https://doi.org/10.1167/iovs.15-17619.
29. Román-Kustas, J., Hoffman, J. B., Reed, J. H., Gonsalves, A. E., Oh, J., Li, L., Hong, S., Jo, K. D., Dana, C. E., Miljkovic, N., Cropek, D. M., & Alleyne, M. (2020). Molecular and Topographical Organization: Influence on Cicada Wing Wettability and Bactericidal Properties. *Advanced Materials Interfaces*, *7*(10), 2000112. https://doi.org/10.1002/admi.202000112

30. Aryaei, A., Jayatissa, A. H., & Jayasuriya, A. C. (2012). Nano and micro mechanical properties of uncross-linked and cross-linked chitosan films. *Journal of the Mechanical Behavior of Biomedical Materials*, *5*(1), 82–89. https://doi.org/10.1016/j.jmbbm.2011.08.006
31. Komiyama, J., Satoh, M., Zhang, WZ. *et al.* State of Water in Swollen Membrane in Relation to Permeability. *Polym J* **23,** 379–388 (1991). https://doi.org/10.1295/polymj.23.379
32. Jason J. Nichols, Loraine T. Sinnott; Tear Film, Contact Lens, and Patient-Related Factors Associated with Contact Lens–Related Dry Eye. *Invest. Ophthalmol. Vis. Sci.* 2006;47(4):1319-1328. doi: https://doi.org/10.1167/iovs.05-1392.
33. M. Young, W.J. Benjamin; CONVENTIONAL HYDROGELS: COMPARISON OF WATER CONTENTS AT ROOM & EYE TEMPERATURES AND CORRELATION WITH OXYGEN PERMEABILITY . Invest. Ophthalmol. Vis. Sci. 2004;45(13):1569.
34. Contact Lenses for Ocular Surface Disease. Clinical Gate. (2015, March 8). https://clinicalgate.com/contact-lenses-for-ocular-surface-disease/.
35. Galas, S., & Copper, L. L. (2016). Oxygen permeability of the pigmented material used in cosmetic daily disposable contact lenses. Clinical Ophthalmology, Volume 10, 2469–2474. https://doi.org/10.2147/opth.s105222
36. Sulley, A., Arnold, K., & Mundorf, M. (2018). Daily disposable and reusable contact lens moduli – Are they really different? Contact Lens and Anterior Eye, 41. https://doi.org/10.1016/j.clae.2018.03.037
37. Xin-Yuan, S., & Tian-Wei, T. (2004). New Contact Lens Based on Chitosan/Gelatin Composites. *Journal of Bioactive and Compatible Polymers*, *19*(6), 467–479. https://doi.org/10.1177/0883911504048410
38. Mi, F.-L., Sung, H.-W., Shyu, S.-S., Su, C.-C., & Peng, C.-K. (2003). Synthesis and characterization of biodegradable TPP/genipin co-crosslinked chitosan gel beads. *Polymer*, *44*(21), 6521–6530. https://doi.org/10.1016/s0032-3861(03)00620-7
39. Ferreira Tomaz, A., Sobral de Carvalho, S. M., Cardoso Barbosa, R., L Silva, S. M., Sabino Gutierrez, M. A., B de Lima, A. G., & L Fook, M. V. (2018). Ionically Crosslinked Chitosan Membranes Used as Drug Carriers for Cancer Therapy Application. Materials (Basel, Switzerland), 11(10), 2051. https://doi.org/10.3390/ma11102051
40. Tsai, C. C., Huang, R. N., Sung, H. W., & Liang, H. C. (2000). In vitro evaluation of the genotoxicity of a naturally occurring crosslinking agent (genipin) for biologic tissue fixation. Journal of biomedical materials research, 52(1), 58–65. https://doi.org/10.1002/1097-4636(200010)52:1<58::aid-jbm8>3.0.co;2-0
41. Bhumkar, D. R., & Pokharkar, V. B. (2006). Studies on effect of pH on cross-linking of chitosan with sodium tripolyphosphate: A technical note. *AAPS PharmSciTech*, *7*(2). https://doi.org/10.1208/pt070250
42. Benny D. Freeman, 9 - Mutual Diffusion in Polymeric Systems, Editor(s): Geoffrey Allen, John C. Bevington, Comprehensive Polymer Science and Supplements, Pergamon, 1989, Pages 167-198, ISBN 9780080967011, https://doi.org/10.1016/B978-0-08-096701-1.00227-5.
43. Muzzarelli, R., El Mehtedi, M., Bottegoni, C., Aquili, A., & Gigante, A. (2015). Genipin-Crosslinked Chitosan Gels and Scaffolds for Tissue Engineering and Regeneration of Cartilage and Bone. Marine Drugs, 13(12), 7314–7338. https://doi.org/10.3390/md13127068

44. Tomaz, Alecsandra & Carvalho, Sandra & Barbosa, Rossemberg & Silva, Suédina & Gutierrez, Marcos & Lima, Antônio & Lia Fook, Marcus. (2018). Ionically Crosslinked Chitosan Membranes Used as Drug Carriers for Cancer Therapy Application. Materials. 11. 2051. 10.3390/ma11102051.
45. Harding, M. W., Marques, L. L. R., Howard, R. J., & Olson, M. E. (2009). Can filamentous fungi form biofilms? *Trends in Microbiology*, *17*(11), 475–480. https://doi.org/10.1016/j.tim.2009.08.007
46. Prados-Rosales, R., Luque-Garcia, J.L., Martínez-López, R., Gil, C. and Di Pietro, A. (2009), The *Fusarium oxysporum* cell wall proteome under adhesion-inducing conditions. Proteomics, 9: 4755-4769. https://doi.org/10.1002/pmic.200800950
47. Van Dijck P, Sjollema J, Cammue BP, Lagrou K, Berman J, d'Enfert C, Andes DR, Arendrup MC, Brakhage AA, Calderone R, Cantón E, Coenye T, Cos P, Cowen LE, Edgerton M, Espinel-Ingroff A, Filler SG, Ghannoum M, Gow NAR, Haas H, Jabra-Rizk MA, Johnson EM, Lockhart SR, Lopez-Ribot JL, Maertens J, Munro CA, Nett JE, Nobile CJ, Pfaller MA, Ramage G, Sanglard D, Sanguinetti M, Spriet I, Verweij PE, Warris A, Wauters J, Yeaman MR, Zaat SAJ, Thevissen K. Methodologies for in vitro and in vivo evaluation of efficacy of antifungal and antibiofilm agents and surface coatings against fungal biofilms. Microb Cell. 2018 Jun 14;5(7):300-326. doi: 10.15698/mic2018.07.638. PMID: 29992128; PMCID: PMC6035839.
48. Shen, Q., Shan, Y., Lü, Y., Xue, P., Liu, Y., & Liu, X. (2019). Enhanced Antibacterial Activity of Poly (dimethylsiloxane) Membranes by Incorporating SiO2 Microspheres Generated Silver Nanoparticles. *Nanomaterials*, *9*(5), 705. https://doi.org/10.3390/nano9050705
49. De-la-Pinta, I., Cobos, M., Ibarretxe, J. et al. Effect of biomaterials hydrophobicity and roughness on biofilm development. J Mater Sci: Mater Med 30, 77 (2019). https://doi.org/10.1007/s10856-019-6281-3
50. Dyavaiah, M., Ramani, R., Chu, D.S. *et al.* Molecular characterization, biofilm analysis and experimental biofouling study of *Fusarium*isolates from recent cases of fungal keratitis in New York State. *BMC Ophthalmol* **7,** 1 (2007). https://doi.org/10.1186/1471-2415-7-1
51. Molladavoodi, S., Robichaud, M., Wulff, D., & Gorbet, M. (2017). Corneal epithelial cells exposed to shear stress show altered cytoskeleton and migratory behaviour. Plos One, 12(6). doi: 10.1371/journal.pone.0178981
52. King-Smith PE, Hinel EA, Nichols JJ. Application of a novel interferometric method to investigate the relation between lipid layer thickness and tear film thinning. Invest Ophthalmol Vis Sci. 2010 May;51(5):2418-23. doi: 10.1167/iovs.09-4387. Epub 2009 Dec 17. PMID: 20019370; PMCID: PMC3259007.